

Quantum Theory of Reactive Scattering in Phase Space

Arseni Goussev^{1*}, Roman Schubert^{1†}, Holger Waalkens^{1,2‡}, and Stephen Wiggins^{1§}

May 30, 2018

¹ School of Mathematics, University of Bristol, University Walk, Bristol BS8 1TW, UK

² Johann Bernoulli Institute for Mathematics and Computer Sciences, University of Groningen, PO Box 407, 9700 AK Groningen, The Netherlands

Abstract

We review recent results on quantum reactive scattering from a phase space perspective. The approach uses classical and quantum versions of Poincaré-Birkhoff normal form theory and the perspective of dynamical systems theory. Over the past ten years the classical normal form theory has provided a method for realizing the phase space structures that are responsible for determining reactions in high dimensional Hamiltonian systems. This has led to the understanding that a new (to reaction dynamics) type of phase space structure, a *normally hyperbolic invariant manifold* (or, NHIM) is the “anchor” on which the phase space structures governing reaction dynamics are built, e.g. it is the classical analogue of the chemists notion of the “activated complex” and it is essential for the construction of a surface that divides reactants from products which has the “no-recrossing” property for trajectories and minimal flux. The quantum normal form theory provides a method for quantizing these phase space structures through the use of the Weyl quantization procedure. We show that this approach provides a solution of the time-independent Schrödinger equation leading to a (local) S-matrix in a neighborhood of the saddle point governing the reaction. These results can be obtained for any dimensional system for which an accurate normal form can be computed, and it does *not* require numerical solution of the Schrödinger equation or the generation of any classical trajectories. It follows easily that the quantization of the directional flux through the dividing surface with the properties noted above is a flux operator that can be expressed in a “closed form”. Moreover, from the local S-matrix we easily obtain an expression for the cumulative reaction probability (CRP), which is the essential ingredient for the computation of microcanonical reaction rates and thermal reaction rates. Significantly, the expression for the CRP can be evaluated without the need to compute

*Arseni.Goussev@bristol.ac.uk

†Roman.Schubert@bristol.ac.uk

‡H.Waalkens@rug.nl

§S.Wiggins@bristol.ac.uk

classical trajectories. This is a by product of the quantization of classical phase space structures that govern “exact” classical dynamics. The quantization of the NHIM is shown to lead to the activated complex, and the lifetimes of quantum states initialized on the NHIM correspond to the Gamov-Siegert resonances. We apply these results to the collinear nitrogen exchange reaction and a three degree-of-freedom system corresponding to an Eckart barrier coupled to two Morse oscillators. We end by describing some further challenges that are topics of current research, but where some preliminary results are known: corner-cutting tunneling, state-to-state reaction rates, the flux-flux autocorrelation function formalism and the convergence of the quantum normal form. We emphasize that this dynamical systems, phase space approach to quantum reactive scattering through the quantum normal form provides a completely new approach to the computation of the relevant quantum scattering quantities (e.g. CRP, resonances) which shows promise in leading to computationally efficient methods for “high dimensional” systems.

Contents

1	Introduction	3
2	Phase-Space Structures Underlying Reaction Dynamics	6
2.1	Dynamics and phase space structures near the saddle in normal form coordinates	8
2.2	Explicit definition and construction of the phase space structures in the normal form coordinates	11
2.3	The foliation of the reaction region by Lagrangian submanifolds	15
2.4	The Directional Flux Through the Dividing Surface	16
2.5	Effect of Truncation of the Normal Form Algorithm	18
2.6	“Globalizing” the Geometrical Structures in the Reaction Region . . .	18
3	Quantum Normal Form Representation of the Activated Complex	20
4	The Cumulative Reaction Probability	26
4.1	General Formulation	26
4.2	Nitrogen Exchange Reaction	28
4.3	A 3 DoF Reactive System	31
5	Gamov-Siegert Resonances	34
6	Further Challenges	36
6.1	Corner-Cutting Tunneling	36
6.2	State-to-State Reaction Rates	37
6.3	Flux-Flux Autocorrelation Function Formalism	38
6.4	Convergence of Quantum Normal Form	41
7	Conclusions	44

A The Normal Form Algorithm: Classical and Quantum	44
A.1 The classical normal form algorithm	45
A.2 The quantum normal form algorithm	49

1 Introduction

Over the past fifty years the computation of quantities describing quantum reactive scattering processes has been a topic of great interest in the chemistry and physics community, see the Perspective article of Miller [1] for background and history. The interest in this topic continues to grow as a result of the need to include quantum effects in order to understand the behavior of certain biomolecules and molecular materials ([2]). These contemporary applications are concerned with “large systems”, and quantum mechanical calculations are notorious for their consumption of computational resources as the number of degrees-of-freedom grows. As noted in [3], the Nobel Prize winner Walter Kohn has identified the problem as the exponential wall of difficulty when one tries to perform numerical calculations in the traditional manner using the rules of quantum mechanics. In this review we discuss a new (phase space) approach to quantum reactive scattering that allows us to bypass the traditional computational difficulties for certain types of physically relevant quantities.

Our purpose here is not to review the entire field of quantum reactive scattering. That would be a huge task that is beyond the scope of this review. Rather, we begin by describing the standard quantities that are computed to describe quantum reactive scattering processes and the issues associated with their computation. Our description follows the excellent review of Miller [4].

The quantity that contains a great deal of detailed information about a particular quantum reactive scattering process is the **S**-matrix. The **S**-matrix, $\{S_{n_p, n_r}(E, J)\}$ as a function of total energy E and total angular momentum J , can be obtained by solving the Schrödinger equation with scattering boundary conditions. From the **S**-matrix state-to-state differential scattering cross-sections can be computed as follows:

$$\sigma_{n_p \leftarrow n_r}(\theta, E) = |(2ik_{n_r})^{-1} \sum_J (2J+1) d_{m_p, m_r}^J(\theta) S_{n_p, n_r}(E, J)|^2, \quad (1.1)$$

where n_r (n_p) labels the reactant (product) rotational and vibrational states, θ is the scattering angle between the relative velocity vectors of reactants and products, m_r (m_p) is the projection of total angular momentum onto the relative velocity vector of the reactants (products) and $d_{m_p, m_r}^J(\theta)$ is the Wigner rotation matrix.

For many chemical reactions a sufficient description is provided by the *rate constant*, either the canonical rate constant characterized by the temperature, $k(T)$, or the microcanonical rate constant characterized by the total energy, $k(E)$. These rate constants can be obtained using appropriate averages of the state-to-state differential cross sections. This averaging process yields the *cumulative reaction probability* (CRP):

$$\mathcal{N}(E) = \sum_J (2J+1) \sum_{n_p, n_r} |S_{n_p, n_r}(E, J)|^2, \quad (1.2)$$

which is used to compute the microcanonical and canonical rate constants, as follows

$$k(E) = [2\pi\hbar\rho_r(E)]^{-1}\mathcal{N}(E), \quad (1.3)$$

$$k(T) = [2\pi\hbar Q_r(T)]^{-1} \int_{-\infty}^{\infty} dE e^{-\beta E} \mathcal{N}(E). \quad (1.4)$$

where $\beta = (kT)^{-1}$, ρ_r is the density of reactant states per unit energy, and Q_r is the reactant partition function per unit volume.

Miller has pointed out ([4]) that if one is interested only in the rate, then solving the Schrödinger equation to obtain the \mathbf{S} -matrix from which the state-to-state differential scattering cross section (1.1) is computed, and then subsequently averaged to obtain the cumulative reaction probability (1.2), is an extremely inefficient process in the sense that a great deal of the detailed information obtained through the computation of the \mathbf{S} -matrix is “thrown away” in the averaging process. Instead, Miller [4] discusses a *direct* way to compute $\mathcal{N}(E)$, or $k(T)$, i.e. a method that avoids first computing the \mathbf{S} -matrix, that is also *correct* in the sense that the expressions for $\mathcal{N}(E)$, or $k(T)$ are exact, i.e. no approximations are involved. These expressions are given as follows ([4]):

$$\mathcal{N}(E) = 2\pi\hbar \text{Tr} \left(\delta(E - \hat{H}) \hat{F} P_r \right) \quad (1.5)$$

$$k(T) = Q_r(T)^{-1} \text{Tr} \left(e^{-\beta\hat{H}} \hat{F} P_r \right) \quad (1.6)$$

where \hat{H} is the Hamilton operator, \hat{F} is a flux operator, P_r is the long time limit of the quantum mechanically time evolved Heaviside function, and $\text{Tr}(\cdot)$ denotes the trace operation. Schatz and Ratner [5] point out that there are three possibilities for the use of (1.5) and (1.6) for computing rates. The first is to evaluate the trace of the operators in a basis, the second is to develop semiclassical theories for the rate constants ([6, 2]), and the third is to use the expressions to develop a version of quantum transition state theory ([7]). An alternative approach is to express (1.5) and (1.6) in terms of a form of flux-flux autocorrelation function ([8, 9]), and we discuss this approach in some detail in Section 6.3. A recent survey of methods for computing reaction rates is given in [10].

Our approach is firmly rooted in phase space, both the classical and quantum theories. The classical phase space theory forms the “skeleton” on which our quantum theory of reactive scattering in phase space is built. The classical theory of reaction dynamics in phase space is reviewed in Section 2. Certainly there has been earlier work on classical reaction dynamics in phase space. In particular, we note the seminal work of Pechukas, Pollak, Child, and McLafferty from the 1970’s and early 1980’s on two degree-of-freedom Hamiltonian systems ([11, 12, 13, 14, 15, 16, 17, 18]) where the notion of a periodic orbit dividing surface (PODS) was introduced. The PODS bound a two dimensional dividing surface (in the three dimensional energy surface) having the “no-recrossing” property and minimal flux. This work did not generalize to more than two degrees-of-freedom. The generalization has required a new concept—the notion of a *normally hyperbolic invariant manifold*, or NHIM. This

was introduced in the study of phase space transport in Hamiltonian systems with three or more degrees-of-freedom in [19], and was subsequently used in the study of chemical reaction dynamics in [20]. For a d degree-of-freedom Hamiltonian system, the NHIM has the structure of a $2d - 3$ dimensional sphere in the $2d - 1$ dimensional energy surface (so for $d = 2$, the NHIM has the structure of a one dimensional sphere, or periodic orbit). Conceptually, the NHIM is a fundamentally new dynamical object. It is a *manifold* of “saddle type stability” that exists in phase space. In Section 2 we discuss in more detail why this is the mathematical manifestation of the chemists notion of the *activated complex*. Later, it was shown in [21] that the NHIM played the role of the PODS for systems with three or more degrees-of-freedom in the sense that the NHIM is the boundary of a dividing surface having the “no-recrossing” property and minimal flux.

This approach to phase space reaction dynamics for three or more degree-of-freedom Hamiltonian systems did not receive a great deal of applications throughout the 1990’s. One reason for this was that there was not a computational method for realizing NHIMs in specific Hamiltonian systems (with three or more degrees-of-freedom). This changed as a result of the work in [22, 23] where it was shown that the classical Poincaré-Birkhoff normal form theory could be used to compute a coordinate system where the NHIM could be realized, along with a variety of associated phase space structures. Software was developed that enabled the computation of the classical and quantum normal forms, and this allowed the realization of these phase space structures in specific examples¹. This enabled the application of this approach to classical phase space reaction dynamics to HCN isomerization ([24]), computation of the volume of points in an energy surface corresponding to reactive trajectories (the “reactive volume”, [25, 26]), and a realization of Thiele’s [27] notion of “gap times” and reaction rates ([28]).

The generalization of this approach to the quantum setting has been carried out in [29, 30, 31]. The essential tools that make this possible are a quantum mechanical generalization of the classical Poincaré-Birkhoff normal form (described in Appendix A.2) and the Weyl quantization procedure. This firmly establishes a phase space approach to quantum mechanics. Our development and understanding of classical phase space structures associated with reaction dynamics is essential because one sees precisely their quantum mechanical manifestations. For example, in the classical setting the normal form is integrable in a (phase space) neighborhood of a particular saddle point that is relevant to the reaction of interest (in a way that we precisely describe in Section 2). This property is manifested quantum mechanically by yielding a Hamilton operator in (quantum) normal form that factors into separate one-dimensional problems that can be solved exactly. This, in turn, gives rise to a block diagonal \mathbf{S} -matrix that can easily be computed and analyzed. This is described in some detail in Section 4.1. This is a significant result because the implication is if the relevant quantum normal form for a system can be computed, then *regardless of the size of the system*, the \mathbf{S} -matrix can be calculated. In other words, our approach leads to an expression for the \mathbf{S} -matrix that does *not* require a solution of the

¹The software, along with documentation, is freely available for download at <http://lacms.maths.bris.ac.uk/publications/software/index.html>.

Schrödinger equation. In Section 4.1 we show that the classical flux through a dividing surface in phase space having the no-recrossing and minimal flux properties is directly related to the quantum mechanical cumulative reaction probability. We apply this approach to computing the cumulative reaction probability for the collinear nitrogen exchange reaction in Section 4.2 and coupled Eckart-Morse-Morse oscillators in Section 4.3. In Section 5 we show that quantum resonances are related to the time of decay of quantum states initialized on the activated complex. We conclude in Section 6 by considering four developing areas of the theory: “corner cutting” tunneling trajectories, state-to-state reaction rates, the flux-flux autocorrelation formalism, and convergence of the quantum normal form.

2 Phase-Space Structures Underlying Reaction Dynamics

In this section we describe the dynamics and geometry associated with phase space structures governing reaction dynamics. While the emphasis in this review is on quantum mechanics, the phase space structure that we describe forms the classical mechanical “skeleton” on which the quantum mechanical theory is supported. Here we merely summarize the basic results, more details can be found in the references given in the introduction. Our exposition here follows [32].

We consider a Hamiltonian system with d degrees of freedom, phase space coordinates $(\tilde{q}, \tilde{p}) \in \mathbb{R}^d \times \mathbb{R}^d$ and Hamiltonian function H . We assume that $(\tilde{q}_0, \tilde{p}_0)$ is an equilibrium point of Hamilton’s equations which is of saddle-centre-...-centre stability type.² By adding a constant term to the Hamiltonian function (which does not change the dynamics) we can, without loss of generality, assume that $H(\tilde{q}_0, \tilde{p}_0) = 0$. Moreover, for simplicity of exposition, we can assume that the coordinates have been suitably translated so that the relevant equilibrium point $(\tilde{q}_0, \tilde{p}_0)$ is at the origin. For much of the discussion below, we will consider iso-energetic geometrical structures belonging to a single positive energy surface $\Sigma(E) := H^{-1}(E)$ for some constant $E > 0$. However, we note that in [33] essentially the same “picture” of phase space structures governing reaction dynamics has been shown to occur for constant temperature dynamics governed by the Hamiltonian isokinetic thermostat.

We construct geometric structures in a neighborhood of the equilibrium point. We emphasize that by “neighborhood” we mean a neighborhood in phase space, not just on a fixed energy surface. We denote this neighborhood of the equilibrium point by \mathcal{L} . We will defer until later a discussion of the constraints on the size of this neighborhood; suffice it to say for now that the region is chosen so that a new set of coordinates can be constructed (the normal form coordinates) in which an accurate nonlinear approximation of the Hamiltonian can be expressed (the normal

²We will define this more precisely shortly. However, briefly, it means that the matrix associated with the linearization of Hamilton’s equations about this equilibrium point has two real eigenvalues of equal magnitude, with one positive and one negative, and $d - 1$ purely imaginary complex conjugate pairs of eigenvalues. We will assume that the eigenvalues satisfy a nonresonance condition that we will describe more fully in the following.

form Hamiltonian) such that it provides an integrable approximation to the dynamics, as well as an algorithmic procedure for realizing phase space structures to within a given desired accuracy.

Before describing the dynamics in normal form coordinates, as well as the realization of the phase space structures in normal form coordinates that govern “reaction”, i.e. trajectories in a phase space neighborhood of the saddle-centre-...-centre equilibrium point (henceforth, referred to as a “saddle”) we describe the relevant geometric structures that have been developed in the in the references given above. We emphasize that although the normal form procedure provides a specific method for realizing these geometric structures in a given coordinate system, their existence is independent of any specific set of coordinates.

Locally, the $(2d-1)$ -dimensional energy surface $\Sigma(E)$ has the structure of $\mathbb{S}^{2d-2} \times \mathbb{R}$ in the $2d$ -dimensional phase space. The energy surface $\Sigma(E)$ is split locally into two components, “reactants” and “products”, by a $(2d-2)$ -dimensional “dividing surface” that is diffeomorphic to \mathbb{S}^{2d-2} and which we therefore denote by $S_{\text{ds}}^{2d-2}(E)$. The dividing surface that we construct has the following properties:-

- The only way that trajectories can evolve from reactants to products (and vice-versa), without leaving the local region \mathcal{L} , is through $S_{\text{ds}}^{2d-2}(E)$. In other words, initial conditions (ICs) on this dividing surface specify all reacting trajectories.
- The dividing surface that we construct is free of local recrossings; any trajectory which crosses it must leave the neighbourhood \mathcal{L} before it might possibly cross again.
- The dividing surface that we construct minimizes the flux, i.e. the directional flux through the dividing surface will increase upon a generic deformation of the dividing surface (see [21] for the details).

The fundamental phase space building block that allows the construction of a dividing surface with these properties is a particular *Normally Hyperbolic Invariant Manifold* (NHIM) which, for a fixed positive energy E , will be denoted $S_{\text{NHIM}}^{2d-3}(E)$. The NHIM is diffeomorphic to \mathbb{S}^{2d-3} and forms the natural *dynamical equator* of the dividing surface: The dividing surface is split by this equator into $(2d-2)$ -dimensional hemispheres, each diffeomorphic to the open $(2d-2)$ -ball, B^{2d-2} . We will denote these hemispheres by $B_{\text{ds},f}^{2d-2}(E)$ and $B_{\text{ds},b}^{2d-2}(E)$ and call them the “forward reactive” and “backward reactive” hemispheres, respectively. $B_{\text{ds},f}^{2d-2}(E)$ is crossed by trajectories representing “forward” reactions (from reactants to products), while $B_{\text{ds},b}^{2d-2}(E)$ is crossed by trajectories representing “backward” reactions (from products to reactants).

The $(2d-3)$ -dimensional NHIM can be viewed as the energy surface of an (unstable) invariant subsystem which as mentioned above, in chemistry terminology, corresponds to the “activated complex”, which as an oscillating “supermolecule” is located between reactants and products.

The NHIM is of saddle stability type, having $(2d-2)$ -dimensional stable and unstable manifolds $W^s(E)$ and $W^u(E)$ that are diffeomorphic to $\mathbb{S}^{2d-3} \times \mathbb{R}$. Being of

co-dimension ³ one with respect to the energy surface, these invariant manifolds act as separatrices, partitioning the energy surface into “reacting” and “non-reacting” parts as will explain in detail in Sec. 2.2.

2.1 Dynamics and phase space structures near the saddle in normal form coordinates

As mentioned in the previous section, reaction type dynamics are induced by equilibrium points of saddle \times centre \times ... \times centre stability type. These are equilibria for which the matrix associated with the linearisation of Hamilton’s equations have eigenvalues which consist of a pair of real eigenvalues of equal magnitude and opposite sign, $(+\lambda, -\lambda)$, $\lambda \in \mathbb{R}$, and $(d - 1)$ pairs of complex conjugate purely imaginary eigenvalues, $(+i\omega_k, -i\omega_k)$, $\omega_k \in \mathbb{R}$, for $k = 2, \dots, d$.

The phase space structures near equilibria of this type exist independently of a specific coordinate system. However, in order to carry out specific calculations we will need to be able to express these phase space structures in coordinates. This is where Poincaré-Birkhoff normal form theory is used. This is a well-known theory and has been the subject of many review papers and books, see, e.g., [34, 35, 36, 37, 38, 39, 40]. For our purposes it provides an algorithm whereby the phase space structures described in the previous section can be realised for a particular system by means of the normal form transformation which involves making a nonlinear symplectic change of variables,

$$(q, p) = T(\tilde{q}, \tilde{p}), \quad (2.1)$$

into *normal form coordinates*, (q, p) which, in a local neighbourhood \mathcal{L} of the equilibrium point, “decouples” the dynamics into a “reaction coordinate” and “bath modes.” The coordinate transformation T is obtained from imposing conditions on the form of H expressed the new coordinates, (q, p) ,

$$H_{\text{CNF}}(q, p) = H(T^{-1}(q, p)) = H(\tilde{q}, \tilde{p}). \quad (2.2)$$

These conditions are chosen such that H_{CNF} and the resulting equations of motions assume a simple form in which the reaction coordinate and bath modes “decouple”. This decoupling is one way of understanding how we are able to construct the phase space structures, in the normal form coordinates, that govern the dynamics of reaction.

In fact, we will assume that a (generic) non-resonance condition holds between the eigenvalues, namely that

$$k_2\omega_2 + \dots + k_n\omega_d \neq 0 \quad (2.3)$$

³Briefly, the co-dimension of a submanifold is the dimension of the space in which the submanifold exists, minus the dimension of the submanifold. The significance of a submanifold being “co-dimension one” is that it is one less dimension than the space in which it exists. Therefore it can “divide” the space and act as a separatrix, or barrier, to transport.

for all integer vectors $(k_2, \dots, k_d) \in \mathbb{Z}^{d-1}$.⁴ When such a condition holds, the classical normal form procedure, see Appendix A.1, yields an explicit expression for the normalised Hamiltonian H_{CNF} as a function of d integrals of motion:

$$\begin{aligned} H_{\text{CNF}}^{(N)} &= K_{\text{CNF}}^{(N)}(I, J_2, J_3, \dots, J_d) \\ &= E_0 + \lambda I + \sum_{k=2}^d \omega_k J_k + \sum_{n=2}^{\lfloor N/2 \rfloor} \sum_{|\alpha|=n} \kappa_{n,\alpha} I^{\alpha_1} J_2^{\alpha_2} \dots J_d^{\alpha_d}. \end{aligned} \quad (2.4)$$

Note that the normal form is expressed as a polynomial in the action integrals I and J_k , $k = 2, \dots, d$, corresponding to a ‘‘reaction coordinate’’ and $(d - 1)$ ‘‘bath modes’’ respectively. In Eq. (2.4) E_0 denotes the energy of the system at the equilibrium point, and the expansion coefficient $\kappa_{n,\alpha}$ are obtained by the classical normal form algorithm presented in Appendix A; here, $\alpha = (\alpha_1, \dots, \alpha_d)$ with $\alpha_k \in \mathbb{N}_0$ for $k = 1, \dots, d$, and $|\alpha| = \sum_k \alpha_k$. In Appendix A we show that the normal form algorithm generates a polynomial at each step, where the normalization algorithm at a certain order does not modify the normalized terms at lower order. However, in practice it is necessary to stop the algorithm at a given order. In this sense the normal form is an approximation to the original Hamiltonian in a neighborhood of the saddle, which we have denoted by \mathcal{L} . Certainly, it is essential that the approximation is accurate enough to yield useful information. Numerous examples have shown this to be the case, and we discuss this issue more fully in Section 2.5.

The integral, I , corresponds to a ‘‘reaction coordinate’’ (saddle-type DoF):

$$I = q_1 p_1. \quad (2.5)$$

We note that there is an equivalent form of the reaction coordinate:- making the linear symplectic change of variables $q_1 = (P_1 - Q_1)/\sqrt{2}$ and $p_1 = (P_1 + Q_1)/\sqrt{2}$, transforms the above into the following form, which may be more familiar to many readers,

$$I = q_1 p_1 = \frac{1}{2} (P_1^2 - Q_1^2). \quad (2.6)$$

Geometrically speaking, one can move freely between these two representations by considering the plane (q_1, p_1) and rotating it by angle $\pi/4$, to give (Q, P) .

The integrals J_k , for $k = 2, \dots, d$, correspond to ‘‘bath modes’’ (centre-type DoF)⁵:

⁴We note that the inclusion of $\pm\lambda$ in a non-resonance condition would be vacuous; one cannot have a resonance of this kind between a real eigenvalue, $\pm\lambda$, and purely imaginary eigenvalues, $\pm i\omega_k$, $k = 2, \dots, d$.

⁵Throughout our work we use, somewhat interchangeably, terminology from both chemical reaction dynamics and dynamical systems theory. This is most noticeable in our reference to the integrals of motion. I is the integral related to reaction, and in the context of dynamical systems theory it is related to hyperbolic behaviour. The term ‘‘reactive mode’’ might also be used to describe the dynamics associated with this integral. The integrals J_2, \dots, J_d describe the dynamics associated with ‘‘bath modes’’. In the context of dynamical systems theory, the dynamics associated with these integrals is referred to as ‘‘center type dynamics’’ or ‘‘center modes’’. A key point here is that integrals of the motion provide us with the

$$J_k = \frac{1}{2} (p_k^2 + q_k^2), \quad k = 2, \dots, d. \quad (2.7)$$

In the new coordinates, Hamilton's equations have a particularly simple form:

$$\begin{aligned} \dot{q}_1 &= \frac{\partial H_{\text{CNF}}}{\partial p_1} = \Lambda_1(I, J_2, \dots, J_d)q_1, \\ \dot{p}_1 &= -\frac{\partial H_{\text{CNF}}}{\partial q_1} = -\Lambda(I, J_2, \dots, J_d)p_1, \\ \dot{q}_k &= \frac{\partial H_{\text{CNF}}}{\partial p_k} = \Omega_k(I, J_2, \dots, J_d)p_k \\ \dot{p}_k &= -\frac{\partial H_{\text{CNF}}}{\partial q_k} = -\Omega_k(I, J_2, \dots, J_d)q_k, \end{aligned} \quad (2.8)$$

for $k = 2, \dots, d$, where we denote

$$\Lambda(I, J_2, \dots, J_d) := \frac{\partial K_{\text{CNF}}(I, J_2, \dots, J_d)}{\partial I} \quad (2.9)$$

$$\Omega_k(I, J_2, \dots, J_d) := \frac{\partial K_{\text{CNF}}(I, J_2, \dots, J_d)}{\partial J_k}, \quad k = 2, \dots, d. \quad (2.10)$$

The integrals provide a natural definition of the term ‘‘mode’’ that is appropriate in the context of reaction, and they are a consequence of the (local) integrability in a neighborhood of the equilibrium point of saddle-centre-...-centre stability type. Moreover, the expression of the normal form Hamiltonian in terms of the integrals provides us a way to partition the ‘‘energy’’ between the different modes. We will provide examples of how this can be done in the following.

The normal form transformation T in (2.1) can be computed in an algorithmic fashion. One can give explicit expression for the phase space structures discussed in the previous section in terms of the normal form coordinates, (q, p) . This way the phase space structures can be constructed in terms on the normal form coordinates, (q, p) , and for physical interpretation, transformed back to the original ‘‘physical’’ coordinates, (\tilde{q}, \tilde{p}) , by the inverse of the transformation T .⁶

In summary, the ‘‘output’’ of the normal form algorithm is the following:

- A symplectic transformation $T(\tilde{q}, \tilde{p}) = (q, p)$, and its inverse $T^{-1}(q, p) = (\tilde{q}, \tilde{p})$, that relate the normal form coordinates (q, p) to the original ‘‘physical’’ coordinates (\tilde{q}, \tilde{p}) .

natural way of defining and describing the physical notion of a ‘‘mode’’. The nature of the mode is defined in the context of the specific application (i.e. chemical reactions) or, in the context of dynamical systems theory, through its stability properties (i.e. hyperbolic or centre).

⁶The original coordinates (\tilde{q}, \tilde{p}) typically have an interpretation as configuration space coordinates and momentum coordinates. The normal form coordinates (q, p) , in general, do not have such a physical interpretation since both q and p are nonlinear functions of both \tilde{q} and \tilde{p} .

- An expression for the normalized Hamiltonian: in the form, H_{CNF} , in terms of the normal form coordinates (q, p) , and in the form K_{CNF} , in terms of the integrals (I, J_2, \dots, J_d) .
- Explicit expressions for the integrals of motion I and J_k , $k = 2, \dots, d$, in terms of the original “physical” coordinates by means of the symplectic transformation $T(\tilde{q}, \tilde{p}) = (q, p)$.

2.2 Explicit definition and construction of the phase space structures in the normal form coordinates

As indicated in the previous section it is straightforward to construct the local phase space objects governing “reaction” in the normal form coordinates, (q, p) . In this section, we will define the various structures in the normal form coordinates and discuss briefly the consequences for the original dynamical system.

The structure of an energy surface near a saddle point: For $E < 0$, the energy surface consists of two disjoint components. The two components correspond to “reactants” and “products.” The top panel of Fig. 1 shows how the two components project to the various planes of the normal form coordinates. The projection to the plane of the saddle coordinates (q_1, p_1) is bounded away from the origin by the two branches of the hyperbola, $q_1 p_1 = I < 0$, where I is given implicitly by the energy equation with the centre actions J_k , $k = 2, \dots, d$, set equal to zero: $K_{\text{CNF}}(I, 0, \dots, 0) = E < 0$. The projections to the planes of the centre coordinates, (q_k, p_k) , $k = 2, \dots, d$, are unbounded.

At $E = 0$, the formerly disconnected components merge (the energy surface bifurcates), and for $E > 0$, the energy surface has locally the structure of a spherical cylinder, $\mathbb{S}^{2d-2} \times \mathbb{R}$. Its projection to the plane of the saddle coordinates now includes the origin. In the first and third quadrants it is bounded by the two branches of the hyperbola, $q_1 p_1 = I > 0$, where I is again given implicitly by the energy equation with all centre actions equal to zero, but now with an energy greater than zero: $K_{\text{CNF}}(I, 0, \dots, 0) = E > 0$. The projections to the planes of the centre coordinates are again unbounded. This is illustrated in the bottom panel of Fig. 1.

The dividing surface, and reacting and nonreacting trajectories: On an energy surface with $E > 0$, we define the dividing surface by $q_1 = p_1$. This gives a $(2d-2)$ -sphere which we denote by $S_{\text{ds}}^{2d-2}(E)$. Its projection to the saddle coordinates simply gives a line segment through the origin which joins the boundaries of the projection of the energy surface, as shown in Fig. 2. The projections of the dividing surface to the planes of the centre coordinates are bounded by circles $(p_k^2 + q_k^2)/2 = J_k$, $k = 2, \dots, d$, where J_k is determined by the energy equation with the other centre actions, J_l , $l \neq k$, and the saddle integral, I , set equal to zero. The dividing surface divides the energy surface into two halves, $p_1 - q_1 > 0$ and $p_1 - q_1 < 0$, corresponding to reactants and products.

As mentioned above, trajectories project to hyperbolae in the plane of the saddle coordinates, and to circles in the planes of the centre coordinates. The sign of I determines whether a trajectory is nonreacting or reacting, see Fig. 2. Trajectories

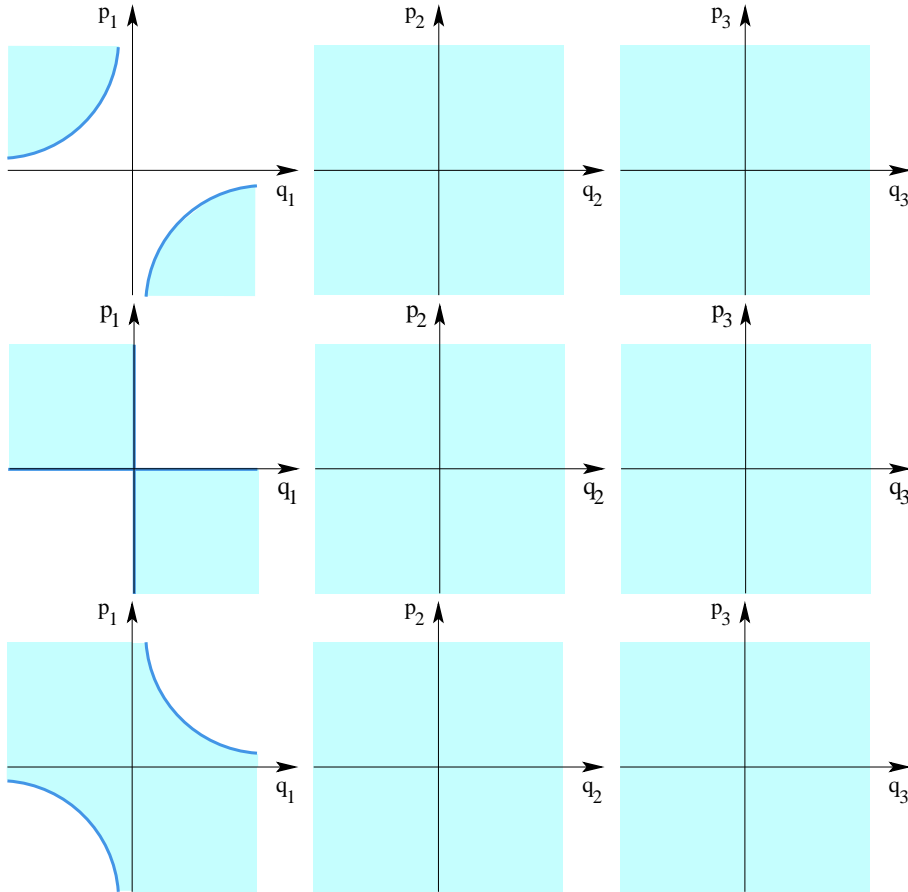


Figure 1: Projection of energy surfaces (turquoise regions) to the planes of the normal form coordinates. The energy surface have energy $E < 0$ (top panel), $E = 0$ (middle panel), $E > 0$ (bottom panel).

which have $I < 0$ are nonreactive and for one branch of the hyperbola $q_1 p_1 = I$ they stay on the reactants side and for the other branch they stay on the products side; trajectories with $I > 0$ are reactive, and for one branch of the hyperbola $q_1 p_1 = I$ they react in the forward direction, i.e., from reactants to products, and for the other branch they react in the backward direction, i.e., from products to reactants. The projections of reactive trajectories to the planes of the centre coordinates are always contained in the projections of the dividing surface. In this, and other ways, the geometry of the reaction is highly constrained. There is no analogous restriction on the projections of nonreactive trajectories to the centre coordinates.

The normally hyperbolic invariant manifold (NHIM) and its relation to the “activated complex”: On an energy surface with $E > 0$, the NHIM is given by $q_1 = p_1 = 0$. The NHIM has the structure of a $(2d - 3)$ -sphere, which we denote by $S_{\text{NHIM}}^{2d-3}(E)$. The NHIM is the equator of the dividing surface; it divides it into two “hemispheres”: the *forward dividing surface*, which has $q_1 = p_1 > 0$, and the

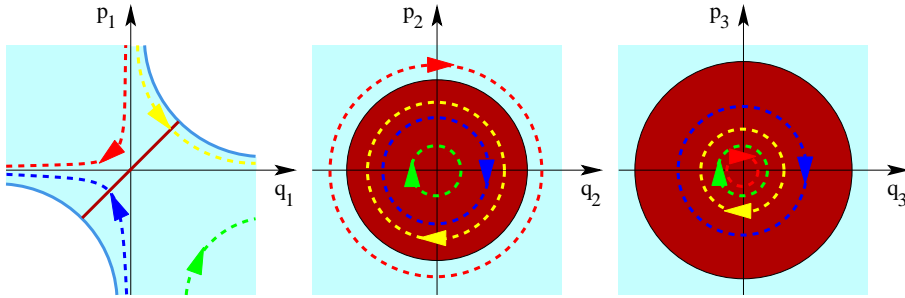


Figure 2: Projection of the dividing surface and reacting and nonreacting trajectories to the planes of the normal form coordinates. In the plane of the saddle coordinates, the projection of the dividing surface is the dark red diagonal line segment, which has $q_1 = p_1$. In the planes of the centre coordinates, the projections of the dividing surface are the dark red discs. Forward and backward reactive trajectories (yellow and blue) project to the first and third quadrant in the plane of the saddle coordinates, respectively, and pass through the dividing surface. The red and green curves mark nonreactive trajectories on the reactant side ($p_1 - q_1 > 0$), and on the product side ($p_1 - q_1 < 0$), of the dividing surface, respectively. The turquoise regions indicate the projections of the energy surface.

backward dividing surface, which has $q_1 = p_1 < 0$. The forward and backward dividing surfaces have the structure of $(2d - 2)$ -dimensional balls, which we denote by $B_{\text{ds},f}^{2d-2}(E)$ and $B_{\text{ds},b}^{2d-2}(E)$, respectively. All forward reactive trajectories cross $B_{\text{ds},f}^{2d-2}(E)$; all backward reactive trajectories cross $B_{\text{ds},b}^{2d-2}(E)$. Since $q_1 = p_1 = 0$ in the equations of motion (2.8) implies that $\dot{q}_1 = \dot{p}_1 = 0$, the NHIM is an invariant manifold, i.e., trajectories started in the NHIM stay in the NHIM for all time. The system resulting from $q_1 = p_1 = 0$ is an invariant subsystem with one degree of freedom less than the full system. In fact, $q_1 = p_1 = 0$ defines the centre manifold associated with the saddle-centre-...-centre equilibrium point, and the NHIM at an energy E greater than the energy of the equilibrium point is given by the intersection of the centre manifold with the energy surface of this energy E [23, 21].

This invariant subsystem with one degree of freedom less than the full system is the “activated complex” (in phase space), located between reactants and products. The NHIM can be considered to be the energy surface of the activated complex. In particular, all trajectories in the NHIM have $I = 0$.

The equations of motion (2.8) also show that $\dot{p}_1 - \dot{q}_1 < 0$ on the forward dividing surface $B_{\text{ds},f}^{2d-2}(E)$, and $\dot{p}_1 - \dot{q}_1 > 0$ on the backward dividing surface $B_{\text{ds},b}^{2d-2}(E)$. Hence, except for the NHIM, which is an invariant manifold, the dividing surface is everywhere transverse to the Hamiltonian flow. This means that a trajectory, after having crossed the forward or backward dividing surface, $B_{\text{ds},f}^{2d-2}(E)$ or $B_{\text{ds},b}^{2d-2}(E)$, respectively, must leave the neighbourhood of the dividing surface before it can possibly cross it again. Indeed, such a trajectory must leave the local region in which the normal form is valid before it can possibly cross the dividing surface again.

The NHIM has a special structure: due to the conservation of the centre actions,

it is filled, or *foliated*, by invariant $(d - 1)$ -dimensional tori, \mathbb{T}^{d-1} . More precisely, for $d = 3$ degrees of freedom, each value of J_2 implicitly defines a value of J_3 by the energy equation $K_{\text{CNF}}(0, J_2, J_3) = E$. For three degrees of freedom, the NHIM is thus foliated by a one-parameter family of invariant 2-tori. The end points of the parameterization interval correspond to $J_2 = 0$ (implying $q_2 = p_2 = 0$) and $J_3 = 0$ (implying $q_3 = p_3 = 0$), respectively. At the end points, the 2-tori thus degenerate to periodic orbits, the so-called *Lyapunov periodic orbits*.

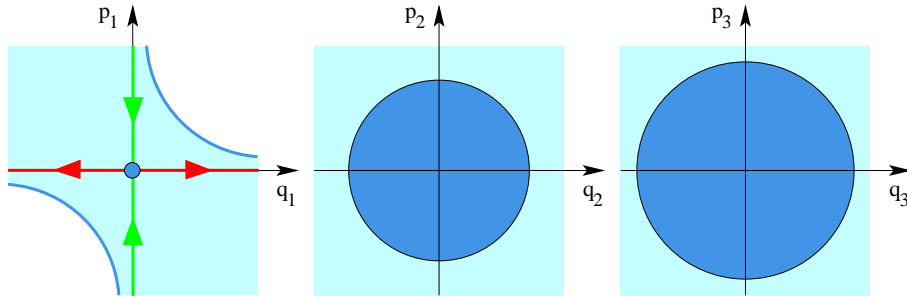


Figure 3: The projection of the NHIM and the local parts of its stable and unstable manifolds, $W^s(E)$ and $W^u(E)$, to the planes of the normal form coordinates. In the plane of the saddle coordinates, the projection of the NHIM is the origin marked by the blue bold point, and the projection of $W^s(E)$ and $W^u(E)$ are the p_1 -axis and q_1 -axis, respectively. $W^s(E)$ consists of the forward and backward branches $W_f^s(E)$ and $W_b^s(E)$, which have $p_1 > 0$ and $p_1 < 0$, respectively; $W^u(E)$ consists of $W_f^u(E)$ and $W_b^u(E)$, which have $q_1 > 0$ and $q_1 < 0$, respectively. In the plane of the centre coordinates, the projections of the NHIM, $W^s(E)$, and $W^u(E)$ (the blue circular discs) coincide with the projection of the dividing surface in Fig. 2. The turquoise regions mark the projections of the energy surface.

The stable and unstable manifolds of the NHIM forming the phase space conduits for reactions: Since the NHIM is of saddle stability type, it has stable and unstable manifolds, $W^s(E)$ and $W^u(E)$. The stable and unstable manifolds have the structure of spherical cylinders, $\mathbb{S}^{2d-3} \times \mathbb{R}$. Each of them consists of two branches: the “forward branches”, which we denote by $W_f^s(E)$ and $W_f^u(E)$, and the “backward branches”, which we denote by $W_b^s(E)$ and $W_b^u(E)$. In terms of the normal form coordinates, $W_f^s(E)$ is given by $q_1 = 0$ with $p_1 > 0$, $W_b^s(E)$ is given by $q_1 = 0$ with $p_1 < 0$, and $W_b^u(E)$ is given by $p_1 = 0$ with $q_1 > 0$, $W_f^u(E)$ is given by $p_1 = 0$ with $q_1 < 0$, see Fig. 3. Trajectories on these manifolds have $I = 0$.

Since the stable and unstable manifolds of the NHIM are of one less dimension than the energy surface, they enclose volumes of the energy surface. We call the union of the forward branches, $W_f^s(E)$ and $W_f^u(E)$, the *forward reactive spherical cylinder* and denote it by $W_f(E)$. Similarly, we define the *backward reactive spherical cylinder*, $W_b(E)$, as the union of the backward branches, $W_b^s(E)$ and $W_b^u(E)$.

The reactive volumes enclosed by $W_f(E)$ and $W_b(E)$ are shown in Fig. 4 as their projections to the normal form coordinate planes. In the plane of the saddle

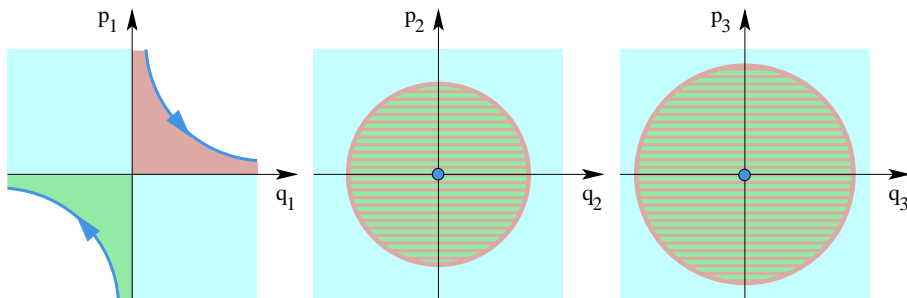


Figure 4: Projections of the reactive volumes enclosed by the forward and backward reactive spherical cylinders, $W_f(E)$ and $W_b(E)$, and the forward and backward reactions paths, to the planes of the normal form coordinates. The volumes enclosed by $W_f(E)$ and $W_b(E)$ project to the dark pink and green regions in the first and third quadrant in the plane of the saddle coordinates, respectively. These volumes project to the dark green/dark pink brindled disks in the planes of the centre coordinates, where their projections coincide with the projection of the NHIM and the dividing surface in Figs. 2 and 3. The forward and backward reaction paths project to the two branches of a hyperbola marked blue in the first and third quadrant in the plane of the saddle coordinates, respectively, and to the origins (bold blue points) in the planes of the centre coordinates. The turquoise regions mark the projections of the energy surface.

coordinates, the reactive volume enclosed by $W_f(E)$ projects to the first quadrant. This projection is bounded by the corresponding hyperbola $q_1 p_1 = I$, with I obtained from $K_{\text{CNF}}(I, 0, \dots, 0) = E$. Likewise, $W_b(E)$ projects to the third quadrant in the (q_1, p_1) -plane. $W_f(E)$ encloses *all* forward reactive trajectories; $W_b(E)$ encloses *all* backward reactive trajectories. *All* nonreactive trajectories are contained in the complement.

2.3 The foliation of the reaction region by Lagrangian submanifolds

The existence of the d integrals of motion, (I, J_2, \dots, J_d) , induce phase space structures which lead to further constraints on the trajectories in addition to the ones described above. In order to describe these structures and the resulting constraints it is useful to introduce the so called *momentum map*, \mathcal{M} [41, 42] which maps a point $(q_1, \dots, q_n, p_1, \dots, p_d)$ in the phase space $\mathbb{R}^d \times \mathbb{R}^d$ to the d integrals evaluated at this point:

$$\mathcal{M} : \mathbb{R}^d \times \mathbb{R}^d \rightarrow \mathbb{R}^d, \quad (q_1, \dots, q_n, p_1, \dots, p_d) \mapsto (I, J_2, \dots, J_d). \quad (2.11)$$

The preimage of a value for the constants of motion (I, J_2, \dots, J_d) under \mathcal{M} is called a *fibre*. A fibre thus corresponds to the common level set of the integrals in phase space.

A point $(q_1, \dots, q_d, p_1, \dots, p_d)$ is called a *regular point* of the momentum map if the linearisation of the momentum map, DM , has full rank d at this point, i.e., if the gradients of the n integrals $I, J_k, k = 2, \dots, d$, with respect to the phase space coordinates (q, p) are linearly independent at this point. If the rank of DM is less than d then the point is called irregular. A fibre is called regular if it consists of regular points only. Otherwise, it is called an irregular fibre. In fact almost all fibres are regular. They are d -dimensional manifolds given by the Cartesian product of an hyperbola $q_1 p_1 = I$ in the saddle plane (q_1, p_1) and $d-1$ circles \mathbb{S}^1 in the centre planes $(q_k, p_k), k = 2, \dots, d$. Since the hyperbola $q_1 p_1 = I$ consists of two branches each of which have the topology of a line \mathbb{R} , the regular fibres consist of two disjoint *toroidal cylinders*, $\mathbb{T}^{d-1} \times \mathbb{R}$, which are the Cartesian products of a $(d-1)$ -dimensional torus and a line. We denote these toroidal cylinders by

$$\Lambda_{I, J_2, \dots, J_d}^+ = \{(q, p) \in \mathbb{R}^{2d} : p_1 q_1 = I, \frac{1}{2}(p_2^2 + q_2^2) = J_2, \dots, \frac{1}{2}(p_d^2 + q_d^2) = J_d, q_1 > 0\} \quad (2.12)$$

and

$$\Lambda_{I, J_2, \dots, J_d}^- = \{(q, p) \in \mathbb{R}^{2d} : p_1 q_1 = I, \frac{1}{2}(p_2^2 + q_2^2) = J_2, \dots, \frac{1}{2}(p_d^2 + q_d^2) = J_d, q_1 < 0\}. \quad (2.13)$$

$\Lambda_{I, J_2, \dots, J_d}^+$ and $\Lambda_{I, J_2, \dots, J_d}^-$ are *Lagrangian manifolds* [43]. The Lagrangian manifolds consists of all trajectories which have the same constants of motion. In particular the Lagrangian manifolds are invariant, i.e. a trajectory with initial condition on a Lagrangian manifold will stay in the Lagrangian manifold for all time. For $I < 0$, the Lagrangian manifolds $\Lambda_{I, J_2, \dots, J_d}^-$ and $\Lambda_{I, J_2, \dots, J_d}^+$ consist of nonreactive trajectories in the reactants resp. products components of the energy surface. For $I > 0$, $\Lambda_{I, J_2, \dots, J_d}^+$ consists of forward reactive trajectories, and $\Lambda_{I, J_2, \dots, J_d}^-$ consists of backward reactive trajectories.

2.4 The Directional Flux Through the Dividing Surface

A key ingredient of transition state theory and the classical reaction rate is the directional flux through the dividing surface defined in Sec. 2.2. Given the Hamiltonian function in normal form expressed as a function of the integrals (2.4), and a fixed energy E above the energy of the saddle-centre-...-centre, E_0 , it is shown in [21] that the directional flux through the dividing surface is given by

$$f(E) = (2\pi)^{d-1} \mathcal{V}(E), \quad (2.14)$$

where $\mathcal{V}(E)$ is the volume in the space of the actions (J_2, \dots, J_d) enclosed by the contour $K_{\text{CNF}}(0, J_2, \dots, J_d) = E$. This is a significant result because it enables the computation of the directional flux *without computing trajectories*. Moreover, it directly connects the directional flux to the NHIM, i.e. the activated complex. In Fig. 5 we illustrate the volume $\mathcal{V}(E)$ for the case of a 3 DoF systems: here $\mathcal{V}(E)$ is

given by the area in the (J_2, J_3) plane enclosed by the light blue line corresponding to the NHIM.

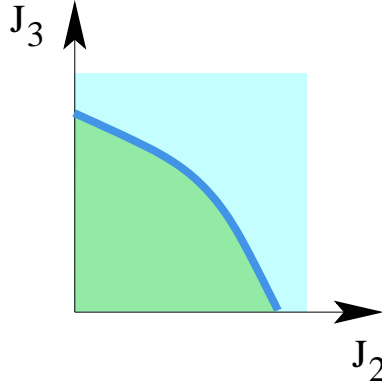


Figure 5: Contour $K_{\text{CNF}}(0, J_2, \dots, J_d) = E$ (blue line) in the space of the centre integrals (J_2, \dots, J_d) for $d = 3$ degrees of freedom. Up to the prefactor $(2\pi)^{d-1}$, the area $\mathcal{V}(E)$ of the enclosed region (marked green) gives the directional flux through the dividing surface, see Equation (2.14). The green region is the projection of the $I > 0$ piece of the energy surface on the (J_2, J_3) -plane.

We also note here that the dimensionless quantity

$$\mathcal{N}_{\text{Weyl}}(E) = \frac{f(E)}{(2\pi\hbar)^{d-1}}, \quad (2.15)$$

where $2\pi\hbar$ is Planck's constant, is Weyl's approximation of the integrated density of states, or equivalently the mean number of quantum states of the activated complex with energies less than or equal to E (see, e.g. [44]). It is shown in [30] that $\mathcal{N}_{\text{Weyl}}(E)$ can be interpreted as the mean number of open quantum "transition channels" at energy E .

In the case where we only take into account the quadratic part of the normal form, or equivalently, if we linearise Hamilton's equations, we have $K_{\text{CNF}}(I, J_2, \dots, J_d) = \lambda I + \sum_{k=2}^d \omega_k J_k$ and the energy surface $K_{\text{CNF}}(0, J_2, \dots, J_d) = E$ encloses a simplex in (J_2, \dots, J_d) whose volume leads to the well-known result [45]

$$f(E) = \frac{E^{d-1}}{(d-1)!} \prod_{k=2}^d \frac{2\pi}{\omega_k}. \quad (2.16)$$

This shows, e.g. that the flux scales with E^{d-1} for energies close to the saddle energy. The key advantage of the normal form coordinates resulting from the normal form algorithm is that it allows one to include the non-linear corrections to (2.16) to any desired order.

2.5 Effect of Truncation of the Normal Form Algorithm

The normalization procedure proceeds via formal power series manipulations whose input is a Taylor expansion of the original Hamiltonian, H , necessarily up to some finite order, N , in homogeneous polynomials. For a particular application, this procedure naturally necessitates a suitable choice of the order, N , for the normalization, after which one must make a restriction to some local region, \mathcal{L} , about the equilibrium point in which the resulting computations achieve some desired accuracy. Hence, the accuracy of the normal form as a power series expansion truncated at order N in a neighborhood \mathcal{L} is determined by comparing the dynamics associated with the normal form with the dynamics of the original system. There are several independent tests that can be carried out to verify accuracy of the normal form. Straightforward tests that we use are the following:

- Examine how the integrals associated with the normal form change on trajectories of the full Hamiltonian (the integrals will be constant on trajectories of the normal form).
- Check invariance of the different invariant manifolds (i.e. the NHIM and its stable and unstable manifolds) with respect to trajectories of the full Hamiltonian.

Both of these tests will require us to use the transformations between the original coordinates and the normal form coordinates. Specific examples where N , \mathcal{L} and accuracy of the normal forms are considered can be found in [24, 46, 25, 47, 26].

2.6 “Globalizing” the Geometrical Structures in the Reaction Region

As we have shown, the normal form transformation to normal form coordinates provides a method for providing a complete understanding of the geometry of reaction dynamics in a neighbourhood \mathcal{L} (in phase space) of the saddle-centre- \dots -centre equilibrium point of Hamilton’s equations. By this, we mean that in the normal form coordinates we can give an explicit equation for the surfaces and, as a result of the “simple” structure of Hamilton’s equations in the normal form coordinates, we can describe precisely the influence of these geometrical structures on trajectories of Hamilton’s equations. In Tab. I we summarize the results obtained this far by providing a list of the different surfaces that control the evolution of trajectories from reactants to products in the neighbourhood \mathcal{L} in Fig. I.

However, it must be kept in mind that all of these surfaces, and associated dynamical phenomena, are only “locally valid” in the neighbourhood \mathcal{L} . The next step is to understand their influence on the dynamics outside of \mathcal{L} , i.e., their influence on the dynamics of reaction throughout phase space in the original coordinates (as opposed to the normal form coordinates). In order to do this we will need the normal form transformation discussed in Appendix A, to order N (where N is determined according to the desired accuracy following the discussion in Section 2.5).

Geometrical Structure	Equation in Normal Form Coordinates
dividing surface, $S_{\text{ds}}^{2d-2}(E)$	$q_1 = p_1$
forward reactive hemisphere, $B_{\text{ds},f}^{2d-2}(E)$	$q_1 = p_1 > 0$
backward reactive hemisphere, $B_{\text{ds},b}^{2d-2}(E)$	$q_1 = p_1 < 0$
NHIM, $S_{\text{NHIM}}^{2d-3}(E)$	$q_1 = p_1 = 0$
stable manifold of the NHIM, $W^s(E)$	$q_1 = 0, p_1 \neq 0$
unstable manifold of the NHIM, $W^u(E)$	$p_1 = 0, q_1 \neq 0$
forward branch of $W^s(E)$, $W_f^s(E)$	$q_1 = 0, p_1 > 0$
backward branch of $W^s(E)$, $W_b^s(E)$	$q_1 = 0, p_1 < 0$
forward branch of $W^u(E)$, $W_f^u(E)$	$p_1 = 0, q_1 > 0$
backward branch of $W^u(E)$, $W_b^u(E)$	$p_1 = 0, q_1 < 0$
forward reactive spherical cylinder $W_f(E) \equiv W_f^s(E) \cup W_f^u(E)$	$p_1 q_1 = 0, p_1, q_1 \geq 0, q_1 \neq p_1$
backward reactive spherical cylinder $W_b(E) \equiv W_b^s(E) \cup W_b^u(E)$	$p_1 q_1 = 0, p_1, q_1 \leq 0, q_1 \neq p_1$

Table I: Table of phase space surfaces influencing reaction dynamics and their representations in normal form coordinates on an energy surface of energy greater than the energy of the saddle equilibrium point.

In Appendix A we discuss the necessary transformations of the original physical coordinates required to transform the Hamiltonian into normal form. In particular, we translate the saddle-centre-...-centre equilibrium point to the origin, we “simplify” the linear part of Hamilton’s equations (what “simplify” precisely means is described in the Appendix), then we iteratively construct a sequence of nonlinear coordinate transformations that successively “simplify” the order 3, 4, ..., N terms of the Hamiltonian according to the algorithm described in Appendix A. We can invert each of these transformations to return from the normal form coordinates to the physical coordinates.

Computation of $W_b^u(E)$ and $W_f^u(E)$: Our approach to computing the stable and unstable manifolds of a NHIM is, in principle, the same as for computing the stable and unstable manifolds of a hyperbolic trajectory (however, the practical implementation of the algorithm in higher dimensions is a different matter and one that deserves much more investigation).

We describe the computation of $W_f^u(E)$ as follows.

- In the normal form coordinates, choose a distribution of initial conditions on the NHIM and displace these initial conditions “slightly” in the direction of the forward branch of $W^u(E)$ ($p_1 = 0, q_1 = \varepsilon > 0, \varepsilon$ “small”).
- Map these initial conditions back into the physical coordinates using the inverse of the normal form transformation.

- Integrate the initial conditions forward in time using Hamilton’s equations in the physical coordinates, for the desired length of time (typically determined by accuracy considerations) that will give the manifold of the desired “size”. Since the initial conditions are in the unstable manifold they will leave the neighbourhood \mathcal{L} in which the normal form transformation is valid (which is why we integrate them in the original coordinates with respect to the original equations of motion).

The backward branch of $W^u(E)$ can be computed in an analogous manner by displacing the initial conditions on the NHIM in the direction of the backward branch of $W^u(E)$ ($p_1 = 0$, $q_1 = \varepsilon < 0$, ε “small”).

Computation of $W_b^s(E)$ and $W_f^s(E)$: The forward and backward branches of $W^s(E)$ can be computed in an analogous fashion, except the initial conditions are integrated *backward* in time.

Practical considerations: By their very definition, invariant manifolds consist of trajectories, and the common way of computing them, and visualizing them, that works well in low dimensions is to integrate a distribution of initial conditions located on the invariant manifold (hence, this illustrates the value of the normal form coordinates and transformation for locating appropriate initial conditions). In high dimensions there are numerical and algorithmic issues that have yet to be fully addressed. How does one choose a mesh on a $2d - 3$ dimensional sphere? As this mesh evolves in time, how does one “refine” the mesh in such a way that the evolved mesh maintains the structure of the invariant manifold?

Examples where this “globalization” of phase space structures in the reaction region has been carried out can be found in [25, 26, 24, 46]. However, there is tremendous scope for future work in this direction, both from the point of view of mathematical and computational techniques, and applications to chemical dynamics.

3 Quantum Normal Form Representation of the Activated Complex

In this section we present an extension of the classical normal form theory to quantum mechanics. Leaving all technical details for Appendix A we only consider here key aspects and results of the theory.

The quantum normal form (QNF) theory⁷ provides an explicit algorithmic procedure that allows one to approximate the Hamiltonian operator \hat{H} , corresponding to a reactive system with a generally *nonintegrable* classical Hamiltonian, by a “simpler” Hamiltonian operator \hat{H}_{QNF} , having an *integrable* classical counterpart. The operator \hat{H}_{QNF} takes the form of a power series expansion in reactive and nonreactive (bath-mode) action operators and the effective Planck’s constant. The (generally infinite)

⁷See Ref. [30] for a comprehensive review of the mathematical theory, or consult Appendix A for a concise summary.

power series can then be terminated at any desired order N dictated by the desired accuracy of the approximation. This leads to an N th order QNF approximation $\hat{H}_{\text{QNF}}^{(N)}$ of the original Hamiltonian \hat{H} :

$$\begin{aligned}\hat{H}_{\text{QNF}}^{(N)} &= K_{\text{QNF}}^{(N)}(\hat{I}, \hat{J}_2, \hat{J}_3, \dots, \hat{J}_d) \\ &= E_0 + \lambda \hat{I} + \sum_{k=2}^d \omega_k \hat{J}_k + \sum_{n=2}^{\lfloor N/2 \rfloor} \sum_{|\alpha|+j=n} \kappa_{n,\alpha,j} \hat{I}^{\alpha_1} \hat{J}_2^{\alpha_2} \dots \hat{J}_d^{\alpha_d} \hbar_{\text{eff}}^j.\end{aligned}\quad (3.1)$$

This approximation holds locally, in the vicinity of a single *equilibrium* point of the Hamiltonian function of the corresponding d -dimensional classical system (see Appendix A for details). It is this equilibrium point whose phase-space neighborhood is traversed by reactive trajectories on their way from the valley of reactants to the valley of products. The equilibrium point is considered to be of saddle-center-...-center stability type, meaning that the $2d \times 2d$ matrix associated with the linearized Hamilton's equations of motion has two real eigenvalues, $\pm\lambda$, and $d-1$ purely imaginary complex conjugate pairs of eigenvalues, $\pm i\omega_k$ with $k = 2, \dots, d$. The linear frequencies ω_k are further assumed to be rationally independent, so that the condition $m_2\omega_2 + \dots + m_d\omega_d = 0$ implies $m_2 = \dots = m_d = 0$ for all integers m_2, \dots, m_d . Other quantities entering Eq. (3.1) include (i) the energy E_0 of the system at the equilibrium point, (ii) parameters $\kappa_{n,\alpha_1,\dots,\alpha_d,j}$ obtained from the QNF expansion procedure, (iii) an effective (scaled) Planck's constant \hbar_{eff} , which in atomic units is given by the inverse of the square root of the reduced mass of the system and plays the role of a "small parameter", (iv) an action integral operator

$$\hat{I} = \frac{1}{2} (\hat{q}_1 \hat{p}_1 + \hat{p}_1 \hat{q}_1) \quad (3.2)$$

corresponding to the reactive mode, and (v) action integral operators

$$\hat{J}_k = \frac{1}{2} (\hat{q}_k^2 + \hat{p}_k^2), \quad k = 2, \dots, d \quad (3.3)$$

of the bath modes. Here, the "position" and "momentum" operators, \hat{q}_k and \hat{p}_k respectively, satisfy the commutation relations

$$[\hat{q}_k, \hat{q}_l] = [\hat{p}_k, \hat{p}_l] = 0, \quad [\hat{q}_k, \hat{p}_l] = i\hbar_{\text{eff}} \delta_{kl}, \quad (3.4)$$

where $k, l = 1, \dots, d$, and δ_{kl} is the Kronecker's delta. The operators $\hat{q}_1, \hat{p}_1, \dots, \hat{q}_d, \hat{p}_d$ are given by the Weyl quantization of classical phase-space coordinates $q_1, p_1, \dots, q_d, p_d$ that in turn are obtained from the original "physical" phase-space coordinates by way of a nonlinear canonical transformation [30]. Thus, \hat{q}_1 and \hat{p}_1 correspond to the reaction coordinate, while \hat{q}_k and \hat{p}_k to the k th bath mode with $k = 2, \dots, d$.

It sometimes proves convenient to work in a phase-space coordinate basis ($Q_1, P_1, q_2, p_2, \dots, q_d, p_d$) (which we further refer as to "QP-basis") that is "rotated" at an angle $\pi/4$ with respect to the basis ($q_1, p_1, q_2, p_2, \dots, q_d, p_d$) (further referred as to "qp-basis"), i.e.,

$$\hat{Q}_1 = \frac{1}{\sqrt{2}} (\hat{q}_1 - \hat{p}_1), \quad \hat{P}_1 = \frac{1}{\sqrt{2}} (\hat{q}_1 + \hat{p}_1). \quad (3.5)$$

In the QP-basis, the action integral operator corresponding to the reaction coordinate reads

$$\hat{I} = \frac{1}{2} \left(\hat{P}_1^2 - \hat{Q}_1^2 \right). \quad (3.6)$$

The main advantage of having the original Hamiltonian \hat{H} approximated by a polynomial in the operators \hat{I} and \hat{J}_k , $k = 2, \dots, d$, is that the eigenstates of the QNF operator $\hat{H}_{\text{QNF}}^{(N)}$ can be chosen to be simultaneously the eigenstates of the operators \hat{I} and \hat{J}_k , whose spectral properties are well known. Indeed,

$$\hat{H}_{\text{QNF}}^{(N)} |I, n_2, \dots, n_d\rangle = E |I, n_2, \dots, n_d\rangle \quad (3.7)$$

with

$$|I, n_2, \dots, n_d\rangle = |\psi_I\rangle \otimes |\psi_{n_2}\rangle \otimes \dots \otimes |\psi_{n_d}\rangle, \quad (3.8)$$

where

$$\hat{I} |\psi_I\rangle = I |\psi_I\rangle, \quad I \in \mathbb{R}, \quad (3.9a)$$

$$\hat{J}_k |\psi_{n_k}\rangle = \hbar_{\text{eff}} (n_k + 1/2) |\psi_{n_k}\rangle, \quad n_k \in \mathbb{N}_0, \quad (3.9b)$$

and

$$E = K_{\text{QNF}}^{(N)} \left(I, \hbar_{\text{eff}} (n_2 + 1/2), \dots, \hbar_{\text{eff}} (n_d + 1/2) \right). \quad (3.10)$$

And, after having explicitly described the eigenstates $|\psi_I\rangle$ and $|\psi_{n_k}\rangle$ of the reaction and bath degrees of freedom respectively, one obtains a complete (approximate) eigensystem for the original reactive scattering problem.

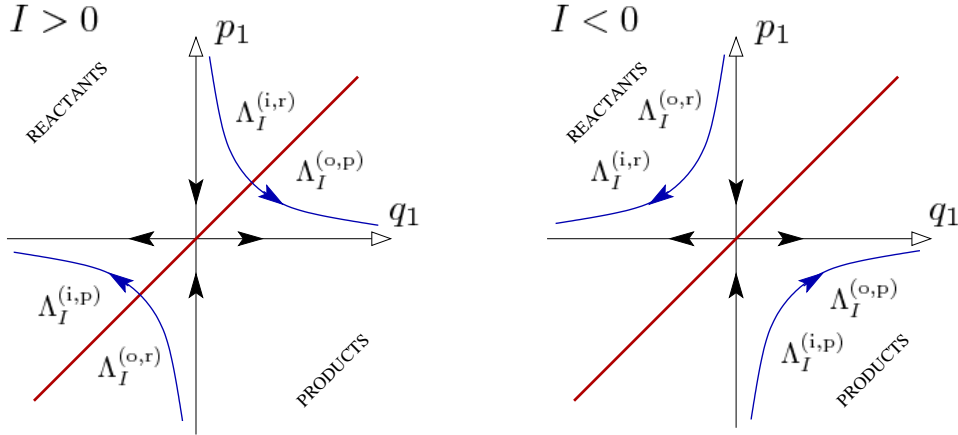


Figure 6: The blue lines show the Lagrangian manifolds $\Lambda_I^{(i,r)}$, $\Lambda_I^{(i,p)}$, $\Lambda_I^{(o,r)}$, and $\Lambda_I^{(o,p)}$ associated with the \hat{I} -eigenstates $|\psi_I^{(i,r)}\rangle$, $|\psi_I^{(i,p)}\rangle$, $|\psi_I^{(o,r)}\rangle$, and $|\psi_I^{(o,p)}\rangle$ respectively. The arrows indicate the classical Hamiltonian vector fields generated by $I = p_1 q_1$. The red thick line corresponds to the dividing surface $s(q_1, p_1) = q_1 - p_1$.

Two independent solutions of Eq. (3.9a), in the q_1 -representation, are given by

$$\langle q_1 | \psi_I^{(o,r)} \rangle = \Theta(-q_1) (-q_1)^{-1/2 + iI/\hbar_{\text{eff}}}, \quad (3.11a)$$

$$\langle q_1 | \psi_I^{(o,p)} \rangle = \Theta(q_1) q_1^{-1/2 + iI/\hbar_{\text{eff}}}, \quad (3.11b)$$

where Θ is the Heaviside step function, the superscript “o” stands for “outgoing to”, and “r” and “p” stand for “reactants” and “products” respectively. The motivation for this notation is clear from viewing the solutions given by Eq. (3.9) as Lagrangian states, i.e., by writing

$$\langle q_1 | \psi_I^{(o,r/p)} \rangle = A_I^{(o,r/p)}(q_1) \exp\left(\frac{i}{\hbar_{\text{eff}}} \varphi_I^{(o,r/p)}(q_1)\right), \quad (3.12)$$

where the purely real amplitude and phase functions are given by

$$A_I^{(o,r/p)}(q_1) = \Theta(\mp q_1) |q_1|^{-1/2}, \quad \varphi_I^{(o,r/p)}(q_1) = I \ln |q_1|, \quad (3.13)$$

respectively. This way one can associate the one-dimensional Lagrangian manifolds

$$\Lambda_I^{(o,r)} = \left\{ (q_1, p_1) = \left(q_1, \frac{d}{dq_1} \varphi_I^{(o,r)}(q_1) \right) = \left(q_1, \frac{I}{q_1} \right) : q_1 < 0 \right\}, \quad (3.14a)$$

$$\Lambda_I^{(o,p)} = \left\{ (q_1, p_1) = \left(q_1, \frac{d}{dq_1} \varphi_I^{(o,p)}(q_1) \right) = \left(q_1, \frac{I}{q_1} \right) : q_1 > 0 \right\} \quad (3.14b)$$

with the states $|\psi_I^{(o,r)}\rangle$ and $|\psi_I^{(o,p)}\rangle$. From the presentation of $\Lambda_I^{(o,r)}$ and $\Lambda_I^{(o,p)}$ in Fig. 6 one sees that for $q_1 \rightarrow -\infty$ the wave function $\langle q_1 | \psi_I^{(o,r)} \rangle$ represents a state outgoing to reactants, and for $q_1 \rightarrow +\infty$ the wave function $\langle q_1 | \psi_I^{(o,p)} \rangle$ represents a state outgoing to products.

Another pair of independent solutions of Eq. (3.9a), $\langle q_1 | \psi_I^{(i,r)} \rangle$ and $\langle q_1 | \psi_I^{(i,p)} \rangle$, corresponding to states “incoming from” reactants and products respectively, is obtained by requiring their momentum representations to be given by

$$\langle p_1 | \psi_I^{(i,r)} \rangle = \langle \psi_I^{(o,p)} | q_1 \rangle \Big|_{q_1=p_1}, \quad \langle p_1 | \psi_I^{(i,p)} \rangle = \langle \psi_I^{(o,r)} | q_1 \rangle \Big|_{q_1=p_1}. \quad (3.15)$$

The corresponding position representations are obtained by way of Fourier transform,

$$\langle q_1 | \cdot \rangle = \frac{1}{\sqrt{2\pi\hbar_{\text{eff}}}} \int e^{iq_1 p_1 / \hbar_{\text{eff}}} \langle p_1 | \cdot \rangle dp_1, \quad (3.16)$$

of $\langle p_1 | \psi_I^{(i,r)} \rangle$ and $\langle p_1 | \psi_I^{(i,p)} \rangle$ defined in Eq. (3.15), namely

$$\langle q_1 | \psi_I^{(i,r)} \rangle = \frac{1}{\sqrt{2\pi\hbar_{\text{eff}}}} \int_0^\infty e^{iq_1 p_1 / \hbar_{\text{eff}}} p_1^{-1/2 - iI/\hbar_{\text{eff}}} dp_1, \quad (3.17a)$$

$$\langle q_1 | \psi_I^{(i,p)} \rangle = \frac{1}{\sqrt{2\pi\hbar_{\text{eff}}}} \int_{-\infty}^0 e^{iq_1 p_1 / \hbar_{\text{eff}}} (-p_1)^{-1/2 - iI/\hbar_{\text{eff}}} dp_1. \quad (3.17b)$$

The integrals in (3.17) are not absolutely convergent, but can be defined as oscillatory integrals. The motivation for defining incoming states according to Eq. (3.15) becomes clear from considering the stationary phase contributions to the integrals (3.17). These come from the p_1 satisfying the stationary phase condition

$$\frac{d}{dp_1} (-I \ln |p_1| + q_1 p_1) = 0, \quad (3.18)$$

i.e., $p_1 = I/q_1$, where $p_1 > 0$ for $\langle q_1 | \psi_I^{(i,r)} \rangle$ and $p_1 < 0$ for $\langle q_1 | \psi_I^{(i,p)} \rangle$. This way one can associate the Lagrangian manifolds

$$\begin{aligned} \Lambda_I^{(i,r)} &= \left\{ (q_1, p_1) = \left(q_1, \frac{I}{q_1} \right) : p_1 > 0 \right\}, \\ \Lambda_I^{(i,p)} &= \left\{ (q_1, p_1) = \left(q_1, \frac{I}{q_1} \right) : p_1 < 0 \right\}. \end{aligned} \quad (3.19)$$

with the incoming states. These manifolds are also shown in Fig. 6. One sees that for $p_1 \rightarrow +\infty$ the wave function $\langle q_1 | \psi_I^{(i,r)} \rangle$ represents a state incoming from reactants, and for $p_1 \rightarrow -\infty$ the wave function $\langle q_1 | \psi_I^{(i,p)} \rangle$ represents a state incoming from products. Finally, calculating the Fourier integrals in Eq. (3.17) [30], one obtains expressions

$$|\psi_I^{(i,r)}\rangle = \frac{e^{i\left(\frac{\pi}{4} - \frac{I}{\hbar_{\text{eff}}}\ln\hbar_{\text{eff}}\right)}}{\sqrt{2\pi}} \Gamma\left(\frac{1}{2} - i\frac{I}{\hbar_{\text{eff}}}\right) \left(e^{\frac{\pi}{2}\frac{I}{\hbar_{\text{eff}}}} |\psi_I^{(o,p)}\rangle - ie^{-\frac{\pi}{2}\frac{I}{\hbar_{\text{eff}}}} |\psi_I^{(o,r)}\rangle \right), \quad (3.20a)$$

$$|\psi_I^{(i,p)}\rangle = \frac{e^{i\left(\frac{\pi}{4} - \frac{I}{\hbar_{\text{eff}}}\ln\hbar_{\text{eff}}\right)}}{\sqrt{2\pi}} \Gamma\left(\frac{1}{2} - i\frac{I}{\hbar_{\text{eff}}}\right) \left(e^{\frac{\pi}{2}\frac{I}{\hbar_{\text{eff}}}} |\psi_I^{(o,r)}\rangle - ie^{-\frac{\pi}{2}\frac{I}{\hbar_{\text{eff}}}} |\psi_I^{(o,p)}\rangle \right), \quad (3.20b)$$

that relate the incoming states to the outgoing ones [48].

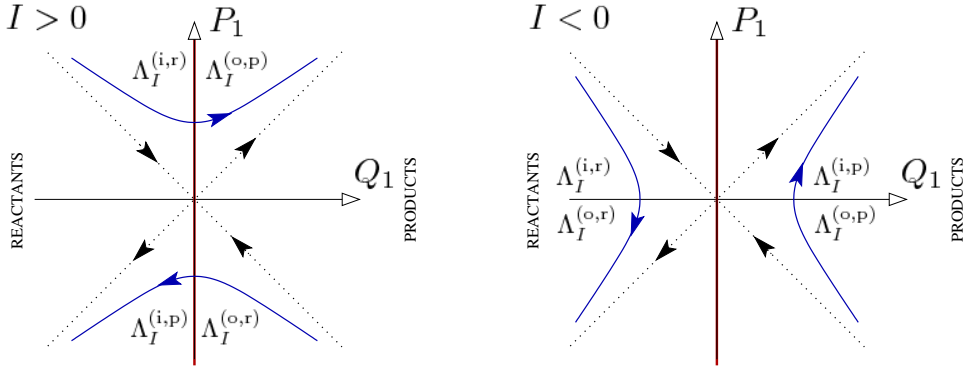


Figure 7: The blue lines show the Lagrangian manifolds $\Lambda_I^{(i,r)}$, $\Lambda_I^{(i,p)}$, $\Lambda_I^{(o,r)}$, and $\Lambda_I^{(o,p)}$ associated with the \hat{I} -eigenstates $|\psi_I^{(i,r)}\rangle$, $|\psi_I^{(i,p)}\rangle$, $|\psi_I^{(o,r)}\rangle$, and $|\psi_I^{(o,p)}\rangle$ respectively. The arrows indicate the classical Hamiltonian vector fields generated by $I = (P_1^2 - Q_1^2)/2$. The red thick line corresponds to the dividing surface $s(Q_1, P_1) = Q_1 = 0$.

The equation for eigenstates of the action operator \hat{I} , Eq. (3.9a), can also be solved in the Q_1 -representation [49, 50]. The two independent solutions are

$$\langle Q_1 | \psi_I^{(i,r)} \rangle = \frac{1}{\pi} (2\hbar_{\text{eff}})^{-\frac{3}{4}} e^{\frac{\pi}{4}\frac{I}{\hbar_{\text{eff}}}} \Gamma\left(\frac{1}{2} - i\frac{I}{\hbar_{\text{eff}}}\right) D_{-\frac{1}{2}+i\frac{I}{\hbar_{\text{eff}}}} \left(e^{-i\frac{\pi}{4}} \sqrt{\frac{2}{\hbar_{\text{eff}}}} Q_1 \right), \quad (3.21a)$$

$$\langle Q_1 | \psi_I^{(i,p)} \rangle = \frac{1}{\pi} (2\hbar_{\text{eff}})^{-\frac{3}{4}} e^{\frac{\pi}{4}\frac{I}{\hbar_{\text{eff}}}} \Gamma\left(\frac{1}{2} - i\frac{I}{\hbar_{\text{eff}}}\right) D_{-\frac{1}{2}+i\frac{I}{\hbar_{\text{eff}}}} \left(e^{i\frac{3\pi}{4}} \sqrt{\frac{2}{\hbar_{\text{eff}}}} Q_1 \right), \quad (3.21b)$$

where D_ν is the parabolic cylinder function of order ν [51]. The outgoing states, $|\psi_I^{(o,r)}\rangle$ and $|\psi_I^{(o,p)}\rangle$, are then obtained from Eq. (3.20). Fig. 7 shows the Lagrangian manifolds $\Lambda_I^{(i,r)}$, $\Lambda_I^{(i,p)}$, $\Lambda_I^{(o,r)}$, and $\Lambda_I^{(o,p)}$ in the (Q_1, P_1) coordinates.

Finally, we note that the incoming and outgoing eigenstates of the \hat{I} operator are orthogonal and satisfy the completeness relations [49, 50]

$$\int_{\mathbb{R}} \left(|\psi_I^{(i,r)}\rangle\langle\psi_I^{(i,r)}| + |\psi_I^{(i,p)}\rangle\langle\psi_I^{(i,p)}| \right) dI = \hat{\mathbb{1}}, \quad (3.22a)$$

$$\int_{\mathbb{R}} \left(|\psi_I^{(o,r)}\rangle\langle\psi_I^{(o,r)}| + |\psi_I^{(o,p)}\rangle\langle\psi_I^{(o,p)}| \right) dI = \hat{\mathbb{1}}, \quad (3.22b)$$

where $\hat{\mathbb{1}}$ stands for the identity operator.

Generally speaking, the q_1 - and Q_1 -representations of the eigenstates of the \hat{I} operator are completely equivalent, and the choice of a representation is usually dictated by a particular problem. For example, in order to determine the total probability flux corresponding to the eigenstates $|\psi_I^{(i,r/p)}\rangle$ through the dividing surface it is convenient to adopt the Q_1 -representation. Indeed, in the QP -basis the operator corresponding to the flux through the dividing surface $s(Q_1, P_1) = Q_1$ is [30]

$$\hat{F} = \frac{i}{\hbar_{\text{eff}}} [\hat{I}, \Theta(\hat{Q}_1)] = \frac{1}{2} \left(\hat{P}_1 \delta(\hat{Q}_1) + \delta(\hat{Q}_1) \hat{P}_1 \right). \quad (3.23)$$

Thus, the expectation value of \hat{F} with respect to the incoming states is given by

$$\begin{aligned} \langle \psi_I^{(i,r/p)} | \hat{F} | \psi_I^{(i,r/p)} \rangle &= \hbar_{\text{eff}} \text{Im} \left(\langle \psi_I^{(i,r/p)} | Q_1 \rangle \frac{d}{dQ_1} \langle Q_1 | \psi_I^{(i,r/p)} \rangle \right) \Big|_{Q_1=0} \\ &= \pm \frac{1}{2\pi\hbar_{\text{eff}}} \frac{1}{1 + \exp(-2\pi I/\hbar_{\text{eff}})}. \end{aligned} \quad (3.24)$$

The operators \hat{J}_k , defined by Eq. (3.3) and corresponding to the action integrals of the bath modes, are the Hamiltonian operators of one-dimensional harmonic oscillators with unit frequency. Therefore, the wave function representing the eigenstates in Eq. (3.9b) are given by

$$\langle q_k | \psi_{n_k} \rangle = \frac{1}{\sqrt{2^{n_k} (n_k!)}} \left(\frac{1}{\pi\hbar_{\text{eff}}} \right)^{1/4} H_{n_k} \left(\frac{q_k}{\sqrt{\hbar_{\text{eff}}}} \right) \exp \left(-\frac{q_k^2}{2\hbar_{\text{eff}}} \right), \quad (3.25)$$

where H_n denotes the n th order Hermite polynomial [51].

Here we note that the quantum normal form Hamiltonian can be interpreted as representing the activated complex. As it has been shown above the QNF Hamiltonian has only continuous spectrum, and so there are no bound states associated with the activated complex. Physically this corresponds to the fact that the activated complex has a finite life time. The latter is determined by the Gamov-Siegert resonances which we discuss in detail in Section 5.

4 The Cumulative Reaction Probability

4.1 General Formulation

The incoming and outgoing eigenstates of \hat{I} defined in Sec. 3 are related to one another by Eq. (3.20). Therefore, each solution $|\psi_I\rangle$ of Eq. (3.9a) can be written as a linear combination of $|\psi_I^{(o,r/p)}\rangle$ or $|\psi_I^{(i,r/p)}\rangle$,

$$|\psi_I\rangle = \alpha_p |\psi_I^{(o,p)}\rangle + \alpha_r |\psi_I^{(o,r)}\rangle = \beta_p |\psi_I^{(i,p)}\rangle + \beta_r |\psi_I^{(i,r)}\rangle. \quad (4.1)$$

These representations are connected by the (one-dimensional) S-matrix,

$$\begin{pmatrix} \alpha_p \\ \alpha_r \end{pmatrix} = \mathcal{S}(I) \begin{pmatrix} \beta_p \\ \beta_r \end{pmatrix}. \quad (4.2)$$

The entries of the S-matrix can be read off directly from Eq. (3.20) yielding

$$\mathcal{S}(I) = \frac{e^{i\left(\frac{\pi}{4} - \frac{I}{\hbar_{\text{eff}}} \ln \hbar_{\text{eff}}\right)}}{\sqrt{2\pi}} \Gamma\left(\frac{1}{2} - i\frac{I}{\hbar_{\text{eff}}}\right) \begin{pmatrix} -ie^{-\frac{\pi}{2}\frac{I}{\hbar_{\text{eff}}}} & e^{\frac{\pi}{2}\frac{I}{\hbar_{\text{eff}}}} \\ e^{\frac{\pi}{2}\frac{I}{\hbar_{\text{eff}}}} & -ie^{-\frac{\pi}{2}\frac{I}{\hbar_{\text{eff}}}} \end{pmatrix}. \quad (4.3)$$

Using the relation $\Gamma(1/2 + iy)\Gamma(1/2 - iy) = \pi/\cosh(\pi y)$ it is easy to see that $\mathcal{S}(I)^*\mathcal{S}(I) = \mathbb{1}$ implying that the S-matrix is unitary.

The transmission coefficient corresponding to the scattering matrix $\mathcal{S}(I)$ reads

$$\mathcal{T}(I) = |\mathcal{S}_{12}(I)|^2 = \frac{e^{\frac{\pi}{\hbar_{\text{eff}}}I}}{e^{\frac{\pi}{\hbar_{\text{eff}}}I} + e^{-\frac{\pi}{\hbar_{\text{eff}}}I}} = \frac{1}{1 + e^{-2\pi\frac{I}{\hbar_{\text{eff}}}}}, \quad (4.4)$$

and the reflection coefficient

$$\mathcal{R}(I) = |\mathcal{S}_{11}(I)|^2 = \frac{e^{-\frac{\pi}{\hbar_{\text{eff}}}I}}{e^{\frac{\pi}{\hbar_{\text{eff}}}I} + e^{-\frac{\pi}{\hbar_{\text{eff}}}I}} = \frac{1}{1 + e^{2\pi\frac{I}{\hbar_{\text{eff}}}}}. \quad (4.5)$$

As required, one has $\mathcal{T}(I) + \mathcal{R}(I) = 1$. The characteristic action scale is given by the effective Planck's constant: \mathcal{T} tends to 1 if $I \gg \hbar_{\text{eff}}$ and to 0 if $I \ll -\hbar_{\text{eff}}$.

In accordance with Eqs. (3.8) and (3.9), the incoming and outgoing scattering states of the d -dimensional reactive system at energy E are given by

$$|\Psi^{(i,r/p)}\rangle = |\psi_I^{(i,r/p)}\rangle \otimes |\psi_{\mathbf{n}}\rangle, \quad (4.6a)$$

$$|\Psi^{(o,r/p)}\rangle = |\psi_I^{(o,r/p)}\rangle \otimes |\psi_{\mathbf{n}}\rangle, \quad (4.6b)$$

where $\mathbf{n} = (n_2, \dots, n_d) \in \mathbb{N}_0^{d-1}$ is a $(d-1)$ -dimensional vector of scattering quantum numbers, and

$$|\psi_{\mathbf{n}}\rangle = |\psi_{n_2}\rangle \otimes \dots \otimes |\psi_{n_d}\rangle \quad (4.7)$$

are the eigenstates of a $(d-1)$ -dimensional harmonic oscillator corresponding to the bath modes. Here, I and \mathbf{n} are not independent, but related by Eq. (3.10). For energies E close to the equilibrium point energy E_0 this equation can be resolved for

the reactive coordinate action, yielding a single valued function $I = I_{\mathbf{n}}(E)$. Then, the S-matrix connecting the scattering states $|\Psi^{(i,r/p)}\rangle$ and $|\Psi^{(o,r/p)}\rangle$ is block-diagonal and given by

$$S_{\mathbf{n},\mathbf{m}}(E) = \delta_{\mathbf{n},\mathbf{m}} \mathcal{S}(I_{\mathbf{n}}(E)), \quad (4.8)$$

where $\delta_{\mathbf{n},\mathbf{m}}$ is the multi-dimensional Kronecker symbol, and $\mathcal{S}(I)$ is given by Eq. (4.3).

The transmission matrix T can be defined as a diagonal matrix with the diagonal elements equal to the modulus squared of the (1, 2)-components of the matrices $\mathcal{S}(I)$ in Eq. (4.8), i.e.,

$$T_{\mathbf{n},\mathbf{m}}(E) = \delta_{\mathbf{n},\mathbf{m}} |\mathcal{S}_{1,2}(I_{\mathbf{n}}(E))|^2 = \delta_{\mathbf{n},\mathbf{m}} \left[1 + \exp \left(- 2\pi \frac{I_{\mathbf{n}}(E)}{\hbar_{\text{eff}}} \right) \right]^{-1}. \quad (4.9)$$

The *cumulative reaction probability* $\mathcal{N}(E)$ is then defined as (see, e.g., [4])

$$\mathcal{N}(E) = \text{Tr} \{ T(E) \}, \quad (4.10)$$

where Tr stands for the trace. Thus, using Eq. (4.9) one obtains

$$\mathcal{N}(E) = \sum_{\mathbf{n}} T_{\mathbf{n},\mathbf{n}}(E) = \sum_{\mathbf{n}} \left[1 + \exp \left(- 2\pi \frac{I_{\mathbf{n}}(E)}{\hbar_{\text{eff}}} \right) \right]^{-1}. \quad (4.11)$$

The cumulative reaction probability $\mathcal{N}(E)$ is the quantum analogue of the classical flux $f(E)$ through the dividing surface or, more precisely, of the dimensionless quantity $f(E)/(2\pi\hbar_{\text{eff}})^{d-1}$. To see this one should consider $\mathcal{N}(E)$ in the semiclassical limit $\hbar_{\text{eff}} \rightarrow 0$, where

$$\lim_{\hbar_{\text{eff}} \rightarrow 0} \left[1 + \exp \left(- 2\pi I / \hbar_{\text{eff}} \right) \right]^{-1} = \Theta(I), \quad (4.12)$$

where Θ is the Heaviside function. This means that the transmission coefficients $T_{\mathbf{n},\mathbf{n}}(E)$ in Eq. (4.11) are characteristic functions, i.e., in the semiclassical limit, $T_{\mathbf{n},\mathbf{n}}(E)$ is 0 or 1 if $I_{\mathbf{n}}(E)$ is negative or positive respectively. This way the cumulative reaction probability can be considered to be a counting function. For a given energy E , it counts how many of the solutions $I_{\mathbf{n}}$ of the equations $K_{\text{QNF}}(I_{\mathbf{n}}, \hbar_{\text{eff}}(n_2 + 1/2), \dots, \hbar_{\text{eff}}(n_d + 1/2)) = E$ with scattering quantum numbers $\mathbf{n} = (n_2, \dots, n_d) \in \mathbb{N}_0^{d-1}$ are positive. In other words, $\mathcal{N}(E)$ can be considered to count the number of open “transmission channels”, where a transmission channel with quantum numbers \mathbf{n} is open if the corresponding transmission coefficient $T_{\mathbf{n},\mathbf{n}}(E)$ is close to 1.

Graphically $\mathcal{N}(E)$ can be interpreted as the number of grid points $(\hbar_{\text{eff}}(n_2 + 1/2), \dots, \hbar_{\text{eff}}(n_d + 1/2))$ in the space of action integrals $(J_2, \dots, J_d) \in [0, \infty)^{d-1}$ that are enclosed by the contour $K_{\text{QNF}}(0, J_2, \dots, J_d) = E$, see Fig. 8. The number of grid points is approximately given by the volume in the space of $(J_2, \dots, J_d) \in [0, \infty)^{d-1}$ enclosed by $K_{\text{QNF}}(0, J_2, \dots, J_d) = E$ divided by \hbar_{eff}^{d-1} . Using the fact that for $\hbar_{\text{eff}} \rightarrow 0$, K_{QNF} becomes the function K_{CNF} which gives the classical energy as a function of the classical integrals (I, J_2, \dots, J_d) we find that the volume in the space of (J_2, \dots, J_d) enclosed by $K_{\text{CNF}}(0, J_2, \dots, J_d) = E$ is given by the classical flux $f(E)$ divided by $(2\pi)^{d-1}$, see Eq. (2.14), and the cumulative reaction probability $\mathcal{N}(E)$ is

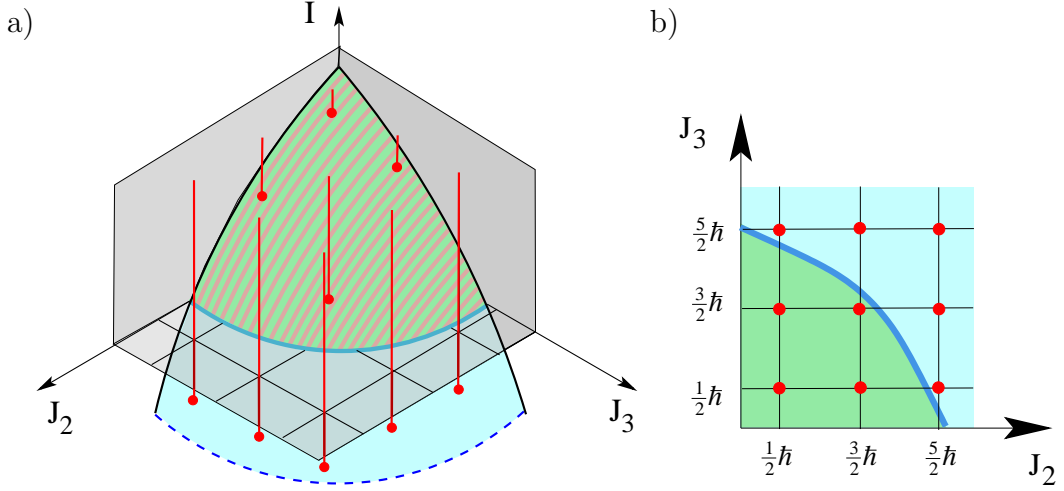


Figure 8: (a) Lines $(I, \hbar_{\text{eff}}(n_2 + 1/2), \dots, \hbar_{\text{eff}}(n_d + 1/2))$, $I \in \mathbb{R}$, $n_k \in \mathbb{N}_0$, $k = 2, \dots, d$, in the space $(I, J_2, \dots, J_d) \in \mathbb{R} \times [0, \infty)^{d-1}$ for $d = 3$ and their intersections with the surface $K_{\text{QNF}}(I, J_2, J_3) = E$. (b) Grid points $(\hbar_{\text{eff}}(n_2 + 1/2), \dots, \hbar_{\text{eff}}(n_d + 1/2))$ in the space (J_2, \dots, J_d) for $d = 3$. The blue line marks the contour $K_{\text{QNF}}(0, J_2, \dots, J_d) = E$. In this plot only the scattering states for which the quantum numbers (n_2, n_3) have the values $(0, 0)$, $(0, 1)$, $(1, 0)$ or $(1, 1)$ correspond to “open transmission channels”, see text.

thus approximately given by $\mathcal{N}_{\text{Weyl}}(E) = f(E)/(2\pi\hbar)^{d-1}$ defined in Eq. (2.15). This way we verify our statement in Sec. 2.4 that $\mathcal{N}_{\text{Weyl}}(E)$ gives the mean number of open transmission channels. In fact, as mentioned in Sec. 2.4, the classical flux $f(E)$ can be considered to be the phase space volume enclosed by the energy contour of energy E of the invariant subsystem which has one degree of freedom less than the full scattering system and which as the so called activated complex is located between reactants and products. $\mathcal{N}_{\text{Weyl}}(E)$ counts how many elementary quantum cells of volume $(2\pi\hbar_{\text{eff}})^{d-1}$ fit into this phase space volume and this way gives the Weyl approximation of the cumulative reaction probability $\mathcal{N}(E)$.

It is important to note here that like the flux in the classical case the cumulative reaction probability is determined by local properties of the Hamilton operator \hat{H} in the neighbourhood of the equilibrium point only.

4.2 Nitrogen Exchange Reaction

In this section we focus on the QNF theory as a tool for computation of the cumulative reaction probability (CRP) and the thermal reaction rate constant. To demonstrate the efficiency and capability of the QNF method and to compare it with other existing methods we follow Ref. [31] and address the CRP and the thermal rate in a collinear triatomic reaction, namely the nitrogen exchange reaction



The collinear version of Eq. (4.13) corresponds to a two degree of freedom reactive system with the Hamiltonian operator of the form

$$\hat{H} \equiv H(\hat{q}_1, \hat{q}_2, \hat{p}_1, \hat{p}_2) = \frac{1}{2} (\hat{p}_1^2 + \hat{p}_2^2) + V(\hat{q}_1, \hat{q}_2), \quad (4.14)$$

where $V(\tilde{q}_1, \tilde{q}_2)$ gives the Born-Oppenheimer potential energy surface, and \tilde{q}_1 and \tilde{q}_2 are the Delves mass-scaled coordinates [52]. The effective Planck's constant is given by $\hbar_{\text{eff}} = \mu^{-1/2}$, where μ is the dimensionless reduced mass of the triatomic system (given in units of the electronic mass). For the case of nitrogen exchange reaction $\mu \approx 1.47 \times 10^4$ yielding $\hbar_{\text{eff}} \approx 8.2 \times 10^{-3}$. We further adopt the London-Eyring-Polanyi-Sato potential energy surface [53] that possess a single saddle point governing the reaction from the asymptotic reactants and products states.

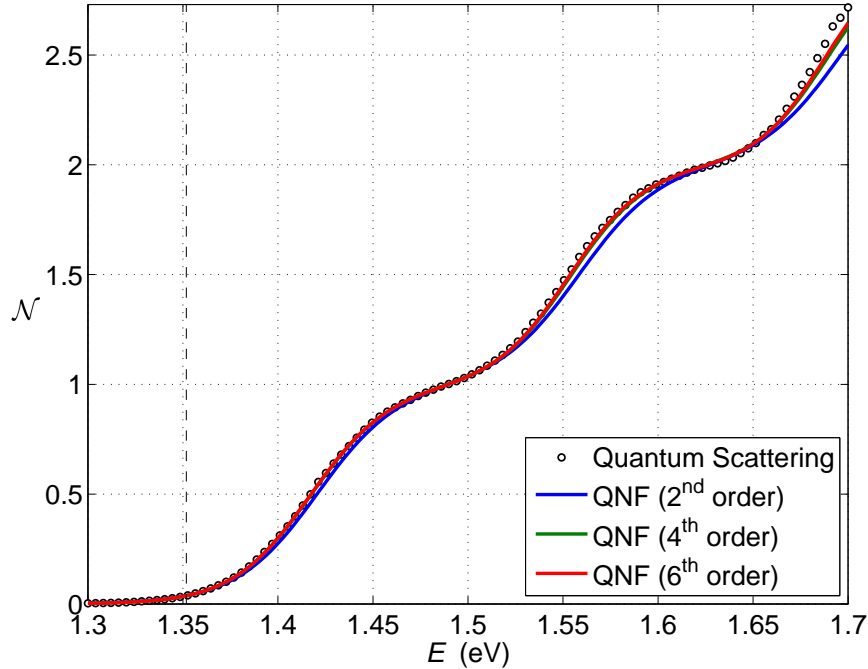


Figure 9: Cumulative reaction probability as a function of the total energy, $\mathcal{N}(E)$, for the collinear nitrogen exchange reaction (4.13). The effective Planck's constant is $\hbar_{\text{eff}} \approx 8.2 \times 10^{-3}$. The $\mathcal{N}(E)$ curves obtained with the 4th and 6th order QNF are essentially indistinguishable for most of the energy range. The vertical dashed line shows the saddle point energy, E_0 .

Following the algorithmic procedure presented in Sec. 3 and Appendix A we compute the N th order approximation

$$\hat{H}_{\text{QNF}}^{(N)} = K_{\text{QNF}}^{(N)}(\hat{I}, \hat{J}_2) \quad (4.15)$$

of the original Hamiltonian operator \hat{H} . The CRP is then given by

$$\mathcal{N}(E) = \sum_{n_2=0}^{\infty} \left[1 + \exp\left(-2\pi \frac{I_{n_2}(E)}{\hbar_{\text{eff}}}\right) \right]^{-1} \quad (4.16)$$

with $I_{n_2}(E)$ solving

$$K_{\text{QNF}}^{(N)}(I, \hbar_{\text{eff}}(n_2 + 1/2)) = E. \quad (4.17)$$

The resulting CPR-vs-energy curves computed for energies in the range between 1.3 and 1.7 eV are shown in Fig. 9. The solid color curves (blue, green, and red) correspond to different orders N of the QNF approximation (2, 4, and 6 respectively). The $\mathcal{N}(E)$ curves obtained with the 4th and 6th order QNF are essentially indistinguishable for most of the energy range; this fact signals the rapid convergence of the QNF expansion for the given value of the effective Planck’s constant. The vertical dashed line shows the saddle point energy, E_0 , of the London-Eyring-Polanyi-Sato potential energy surface.

The circular data points in Fig. 9 represent the “exact” valued of the CRP obtained through the full *reactive quantum scattering* calculation [54, 55]. The latter were performed by integrating the coupled multichannel Schrödinger equation in hyperspherical coordinates [54, 55] from the strong interaction region to the asymptotic reactant and product configurations. The log-derivative matrix method of Manolopoulos and Gray [56] together with the six-step symplectic integrator of McLachlan and Atela [57] was used to integrate the radial Schrödinger equation. It is evident from Fig. 9 that the quantitative agreement of the exact and QNF values of $\mathcal{N}(E)$ well extends up to energies of 1.5 eV.⁸

We finally note that the QNF calculation of the CRP requires significantly less computational time than the corresponding full quantum reactive scattering calculation. For example, the 6th order QNF computation of the nitrogen-exchange CRP curve in Fig. 9 took about 10 minutes on a 2.6 GHz processor, 2 GB RAM computer, while the corresponding full quantum reactive scattering computation took more than 12 hours on the same machine. The QNF approach becomes even more advantageous for treating chemical systems of atoms heavier than nitrogen: the expense of the full quantum computations rapidly grows with the number of asymptotic channels (and, therefore, with mass) [58], while the QNF expansion only becomes more rapidly convergent making the corresponding analysis computationally cheaper.

We now discuss the straightforward extension of the QNF approach to computation of the thermal reaction rate constant, $k(T)$, defined as [59]

$$k(T) = \frac{1}{2\pi Q_r(T)} \int_0^\infty dE \exp\left(-\frac{E}{k_B T}\right) \mathcal{N}(E), \quad (4.18)$$

where T stands for the absolute temperature, $Q_r(T)$ is the partition function of the reactant, and k_B is the Boltzmann constant. To this end, we use the CRP data for the nitrogen exchange reaction, Eq. (4.13), presented in Fig. 9. The data allow us to compute $k(T)$ in the range of temperatures between 600 and 700 K, for which the integrand in the right hand side of Eq. (4.18) is well localized to the energy interval between 1.3 and 1.7 eV. Figure 10 provides a comparison of $k(T)$ calculated from $\mathcal{N}(E)$ obtained using the QNF of orders 2, 4, 6 (color solid lines), and the “exact”, reactive quantum scattering technique (black line with circles). The inset in

⁸It is interesting to note that the QNF curves in Fig. 9 seem to converge to a result that slightly differs from the exact CRP curve at high energies: a small discrepancy starts to show up at energies around 1.5 eV and becomes more pronounced at energies above 1.65 eV. This discrepancy may be attributed to the growing importance of corner-cutting tunneling at high energies. We discuss the phenomenon of the corner-cutting tunneling in relation to the normal form theory in Section 6.1.

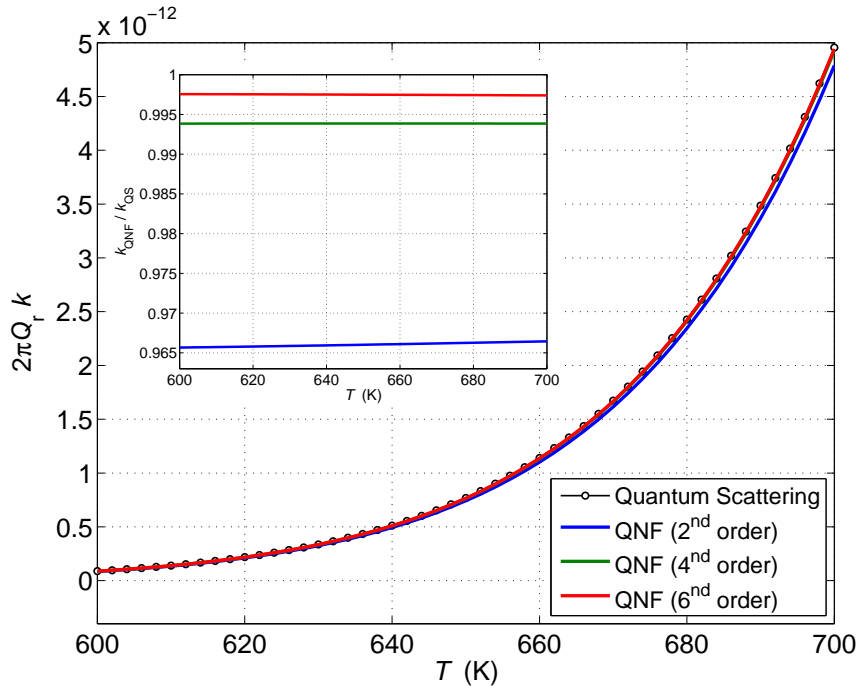


Figure 10: The thermal rate constant (multiplied by the reactant partition function) as a function of temperature for the collinear nitrogen exchange reaction (4.13). The curves obtained with the 4th and 6th order QNF are essentially indistinguishable for most of the energy range. The inset shows the ratio, $k_{\text{QNF}}/k_{\text{QS}}$, of the thermal rate constant computed using the QNF of orders 2, 4, 6, to the one obtained from the quantum scattering data.

the figure shows the ratio, $k_{\text{QNF}}/k_{\text{QS}}$, of the thermal rate computed using the QNF of orders 2, 4, 6, to the one obtained from the quantum scattering data. One can clearly see that the thermal rate constant computed with the QNF method rapidly approaches its exact value as the approximation order N is increased.

4.3 A 3 DoF Reactive System

In order to illustrate the utility of the QNF technique for computation of reaction rates in higher dimensional systems we consider a 3 DoF model system consisting of an Eckart barrier in the (physical) \tilde{q}_1 -direction that is coupled to Morse oscillators in the \tilde{q}_2 -direction and in the \tilde{q}_3 -direction. The Hamiltonian operator is

$$\hat{H} = \frac{1}{2}(\hat{p}_1^2 + \hat{p}_2^2 + \hat{p}_3^2) + V_E(\hat{q}_1) + V_{M;2}(\hat{q}_2) + V_{M;3}(\hat{q}_3) + \epsilon\hat{H}_c. \quad (4.19)$$

Here,

$$V_E(q) = A \frac{\exp((q + q_0)/a)}{1 + \exp((q + q_0)/a)} + B \frac{\exp((q + q_0)/a)}{[1 + \exp((q + q_0)/a)]^2}, \quad (4.20)$$

with positive real parameters a , A , and B , and

$$q_0 = a \ln \frac{B+A}{B-A}, \quad (4.21)$$

is the Eckart potential. For $B > A \geq 0$ it possesses a maximum at $q = 0$; the potential value at the maximum is $V_E(0) = (A+B)^2/(4B)$. The Morse potentials, given by

$$V_{M;k}(q) = D_{e;k} [\exp(-2a_{M;k}q) - 2\exp(-a_{M;k}q)], \quad (4.22)$$

are parametrized by $D_{e;k}$ and $a_{M;k}$, for $k = 2, 3$ respectively. For \hat{H}_c we choose the mutual kinetic coupling

$$\hat{H}_c = \hat{p}_1 \hat{p}_2 + \hat{p}_2 \hat{p}_3 + \hat{p}_3 \hat{p}_1. \quad (4.23)$$

The strength of the coupling is controlled by the parameter ϵ in Eq. (4.19). The vector field generated by the corresponding classical Hamilton function has an equilibrium point at $(\tilde{q}_1, \tilde{q}_2, \tilde{q}_3, \tilde{p}_1, \tilde{p}_2, \tilde{p}_3) = 0$. For $|\epsilon|$ sufficiently small (for given values of parameters of the Eckart and Morse potentials), the equilibrium point is of saddle-centre-centre stability type.

In the uncoupled case, $\epsilon = 0$, it is easy to calculate the exact CRP, $\mathcal{N}_{\text{exact}}(E)$, of the Eckart-Morse-Morse system analytically. Indeed, in accordance with Eq. (4.11),

$$\mathcal{N}_{\text{exact}}(E) = \sum_{n_2=0}^{\infty} \sum_{n_3=0}^{\infty} T_{\text{exact}}(E - E_{M;2,n_2} - E_{M;3,n_3}), \quad (4.24)$$

where T_{exact} denotes the exact transmission coefficient for the Eckart barrier, and is given by [60]

$$T_{\text{exact}}(E) = 1 - \frac{\cosh(2\pi(\alpha - \beta)) + \cosh(2\pi\delta)}{\cosh(2\pi(\alpha + \beta)) + \cosh(2\pi\delta)} \quad (4.25)$$

with

$$\alpha = \frac{1}{2} \sqrt{\frac{E}{C}}, \quad \beta = \frac{1}{2} \sqrt{\frac{E-A}{C}}, \quad \delta = \frac{1}{2} \sqrt{\frac{B-C}{C}}, \quad C = \frac{\hbar_{\text{eff}}^2}{8a^2}. \quad (4.26)$$

In Eq. (4.24), $E_{M;k,n_k}$ (with $k = 2, 3$) are the energy levels of the one-dimensional Morse oscillators,

$$E_{M;k,n_k} = -\frac{1}{2} a_{M;k}^2 \hbar_{\text{eff}}^2 \left(n_k + \frac{1}{2} - \frac{\sqrt{2D_{e;k}}}{a_{M;k} \hbar_{\text{eff}}} \right)^2, \quad n_k = 0, 1, 2, \dots \quad (4.27)$$

The graph of $\mathcal{N}_{\text{exact}}(E)$, obtained from Eqs. (4.24-4.27), is shown by the black oscillatory curve in the top panel of Fig. 11. Here, the parameters for the Eckart potential are $a = 1$, $A = 0.5$, and $B = 5$, the parameters for the Morse potential are $D_{e;2} = 1$, $D_{e;3} = 1.5$, and $a_{M;2} = a_{M;3} = 1$, and the effective Planck's constant $\hbar_{\text{eff}} = 0.1$.

The quantum normal form computation of the CRP for the Eckart-Morse-Morse system gives

$$\mathcal{N}_{\text{QNF}}(E) = \sum_{n_2=0}^{\infty} \sum_{n_3=0}^{\infty} \left[1 + \exp \left(-2\pi \frac{I_{n_2,n_3}(E)}{\hbar_{\text{eff}}} \right) \right]^{-1} \quad (4.28)$$

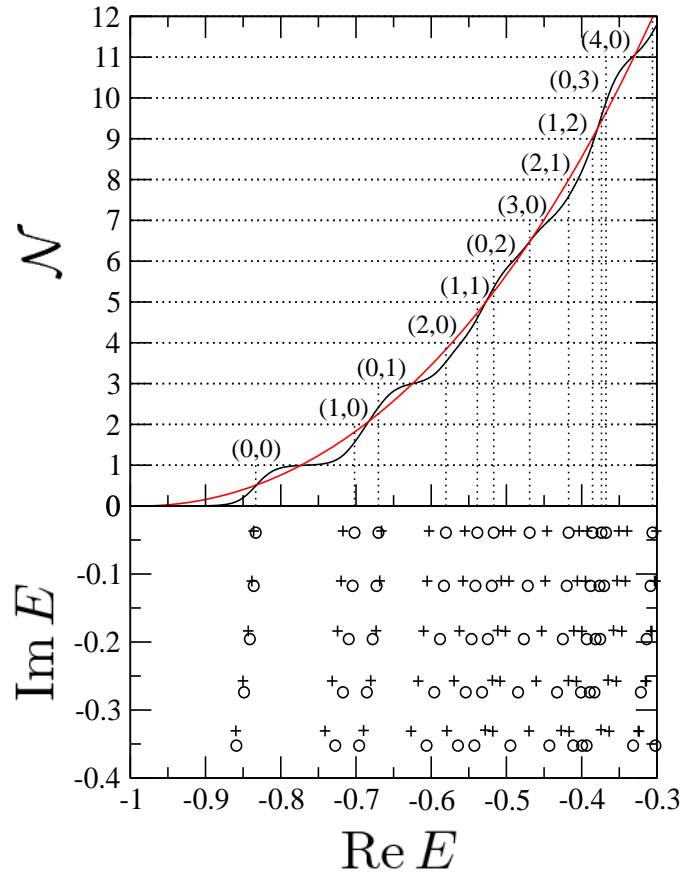


Figure 11: The top panel shows the cumulative reaction probabilities $\mathcal{N}_{\text{exact}}(E)$ (black oscillatory curve) and $\mathcal{N}_{\text{Weyl}}(E)$ (red smooth curve) for the Eckart-Morse-Morse reactive system with the Hamiltonian given by Eq. (4.19) with $\epsilon = 0$. It also shows the quantum numbers (n_2, n_3) of the Morse oscillators that contribute to the quantization steps. The bottom panel shows the resonances in the complex energy plane marked by circles for the uncoupled case $\epsilon = 0$ and by crosses for the strongly coupled case $\epsilon = 0.3$. The parameters for the Eckart potential are $a = 1$, $A = 0.5$, and $B = 5$. The parameters for the Morse potential are $D_{e;2} = 1$, $D_{e;3} = 1.5$, and $a_{M;2} = a_{M;3} = 1$. Also, $\hbar_{\text{eff}} = 0.1$.

with $I_{n_2, n_3}(E)$ solving

$$K_{\text{QNF}}^{(N)}(I, \hbar_{\text{eff}}(n_2 + 1/2), \hbar_{\text{eff}}(n_3 + 1/2)) = E. \quad (4.29)$$

The high quality of the quantum normal form approximation of the cumulative reaction probability is illustrated in Fig. 12, which shows $|\mathcal{N}_{\text{QNF}} - \mathcal{N}_{\text{exact}}|$ as a function of the energy E for different order N of the quantum normal form. It is evident that the CRP computed with the QNF method rapidly approaches its exact value as the approximation order is increased.

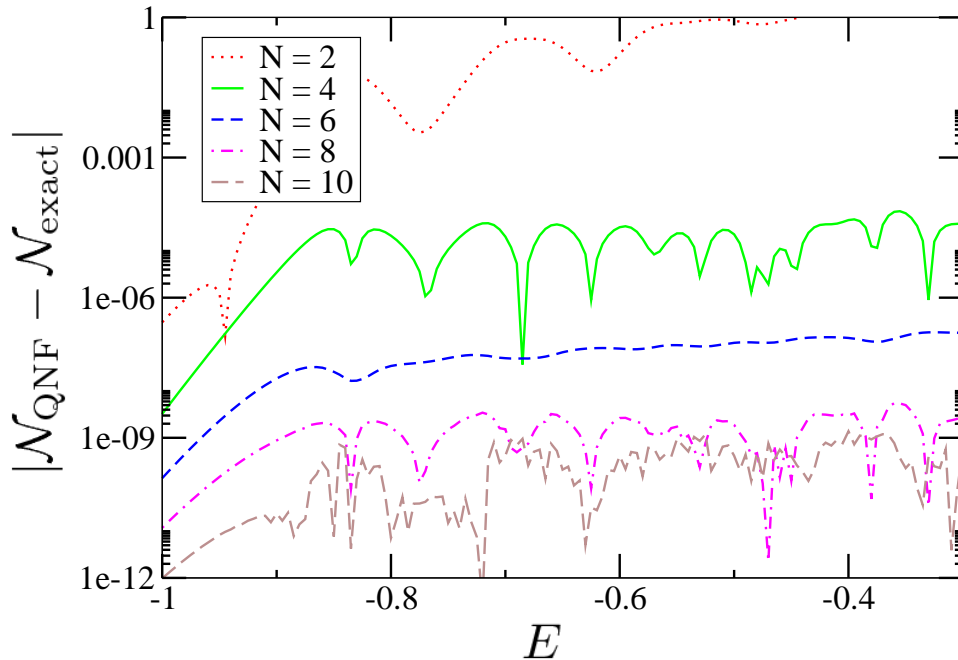


Figure 12: Errors $|\mathcal{N}_{\text{QNF}} - \mathcal{N}_{\text{exact}}|$ for the cumulative reaction probability as a function of energy E of the Eckart-Morse-Morse system for different order N of the quantum normal form.

5 Gamov-Siegert Resonances

As we have discussed in Section 2 in classical mechanics the transition state is represented by a lower dimensional invariant subsystem, the NHIM. In the quantum world, due to Heisenberg's Uncertainty Principle, we cannot localise quantum states entirely on the NHIM, so there can not be any invariant quantum subsystem representing the transition states. Instead we expect a finite lifetime for the transition state. The lifetime of the transition state is determined by the Gamov-Siegert resonances, whose importance in the theory of reaction rates has been emphasized in the literature [61, 62].

Intuitively, a resonance is a complex eigenvalue of a Hamiltonian,

$$\hat{H}|\psi_{res}\rangle = E|\psi_{res}\rangle \quad (5.1)$$

where the imaginary part has to satisfy $\text{Im } E \leq 0$. The time evolution of a resonance state is

$$|\psi_{res}(t)\rangle = e^{-iEt/\hbar_{\text{eff}}}|\psi_{res}\rangle = e^{-\text{Im } Et/\hbar_{\text{eff}}} e^{-i \text{Re } Et/\hbar_{\text{eff}}} |\psi_{res}\rangle$$

and so we see that a resonance state decays in time with lifetime given by

$$T = \frac{\hbar_{\text{eff}}}{|\text{Im } E|}.$$

Notice that since \hat{H} is self-adjoint, a resonant state with complex energy cannot be square integrable.

In order to see how the resonances can be computed from the QNF Hamiltonian, consider first the example of a one-dimensional system described by the Hamilton operator

$$\hat{I} = \frac{1}{2}(\hat{q}\hat{p} + \hat{p}\hat{q}). \quad (5.2)$$

We easily see that $|n\rangle$ defined by $\langle q|n\rangle = q^n$ is a resonance eigenstate

$$\hat{I}|n\rangle = -i\hbar_{\text{eff}}(n + 1/2)|n\rangle. \quad (5.3)$$

with complex eigenvalue

$$E_n = -i\hbar_{\text{eff}}(n + 1/2), \quad n = 0, \dots, N. \quad (5.4)$$

These are the resonances of the operator \hat{I} . Notice that compared to the scattering states $|I\rangle$ which depended on a continuous parameter I , the resonance states are quantized and depend on a discrete parameter $n \in \mathbb{N}_0$. Using this simple example we can now directly determine the resonances and the corresponding resonance states for a Hamilton operator in quantum normal form $\hat{H}_{\text{QNF}} = K_{\text{QNF}}(\hat{I}, \hat{J}_2, \dots, \hat{J}_d)$. Let ψ_{n_k} denote the n_k^{th} harmonic oscillator eigenfunction (see (3.25)). For $n = (n_1, \dots, n_d) \in \mathbb{N}_0^d$, set

$$|n_1, n_2, \dots, n_d\rangle = |n_1\rangle \otimes |\psi_{n_2}\rangle \otimes \dots \otimes |\psi_{n_d}\rangle, \quad (5.5)$$

then we have

$$\begin{aligned} & \hat{H}_{\text{QNF}}|n_1, n_2, \dots, n_d\rangle \\ &= K_{\text{QNF}}(-i\hbar_{\text{eff}}(n_1 + 1/2), \hbar_{\text{eff}}(n_2 + 1/2), \dots, \hbar_{\text{eff}}(n_d + 1/2))|n_1, n_2, \dots, n_d\rangle, \end{aligned} \quad (5.6)$$

and so the resonances of \hat{H}_{QNF} are given by

$$E_{n_1, n_2, \dots, n_d} = K_{\text{QNF}}(-i\hbar_{\text{eff}}(n_1 + 1/2), \hbar_{\text{eff}}(n_2 + 1/2), \dots, \hbar_{\text{eff}}(n_d + 1/2)). \quad (5.7)$$

The bottom panel of Fig. 11 shows the resonances in the complex energy plane that have been computed using Eq. (5.7) for the case of the coupled Eckart-Morse-Morse reactive system discussed in Section 4.3.

The resonances computed from the QNF describe the lifetime of the activated complex. To see this in more detail consider a state localized at time $t = 0$ on the NHIM, i.e., the dependence on the local normal form reaction coordinate q_1 is of the form

$$\langle q_1|\varphi_0\rangle = \frac{1}{(\pi\hbar_{\text{eff}})^{1/4}} e^{-\frac{1}{\hbar_{\text{eff}}}\frac{q_1^2}{2}}. \quad (5.8)$$

which is a minimal uncertainty state. In the bath coordinates we take the state to be given by harmonic oscillator eigenfunctions ψ_{n_k} , so that

$$|\Psi\rangle = |\varphi_0\rangle \otimes |\psi_{n_2}\rangle \otimes \dots \otimes |\psi_{n_d}\rangle \quad (5.9)$$

for some fixed quantum numbers $n_2, \dots, n_d \in \mathbb{N}_0$. Then, expanding $|\Psi\rangle$ into the basis of Eq. (5.5) we obtain the time evolved state

$$|\Psi(t)\rangle = \frac{1}{(\pi\hbar_{\text{eff}})^{1/4}} \sum_{n=0}^{\infty} \frac{1}{n!} \frac{(-1)^n}{(2\hbar_{\text{eff}})^n} e^{-iE_{2n, n_2, \dots, n_d}t/\hbar_{\text{eff}}} |2n, n_2, \dots, n_d\rangle. \quad (5.10)$$

A suitable quantity for measuring the lifetime of a state like (5.9) is the decay of the autocorrelation function

$$|\langle \Psi | \Psi(t) \rangle|^2. \quad (5.11)$$

For the Hamiltonian in quantum normal form the overlap reads

$$\langle \Psi | \Psi(t) \rangle = \left(\frac{2}{\pi} \right)^{1/2} \sum_{n=0}^{\infty} \frac{\Gamma(n+1/2)}{n!} (-1)^n e^{-iE_{2n,n_2,\dots,n_d}t/\hbar_{\text{eff}}}. \quad (5.12)$$

The leading term in this sum for $t \rightarrow \infty$ is given by the smallest resonance with $n = 0$. Hence,

$$|\langle \Psi | \Psi(t) \rangle|^2 \sim 2e^{2\text{Im} E_{0,n_2,\dots,n_d}t/\hbar_{\text{eff}}}, \quad (5.13)$$

and this determines the maximal lifetime of a quantum state of the activated complex, i.e. a state initially localised near the classically invariant subsystem given by the NHIM.

For small \hbar_{eff} the quantum normal form is dominated by its quadratic part and that gives

$$2\text{Im} E_{0,n_2,\dots,n_d}/\hbar_{\text{eff}} \approx -\lambda, \quad (5.14)$$

and therefore for small \hbar_{eff}

$$|\langle \Psi | \Psi(t) \rangle|^2 \sim 2e^{-t\lambda}. \quad (5.15)$$

Thus, the quantum lifetime of the activated complex is in leading order for small \hbar_{eff} given by the reciprocal value of the classical Lyapunov exponent associated with the saddle equilibrium point.

6 Further Challenges

6.1 Corner-Cutting Tunneling

The approach based on normal forms is designed to give an accurate description of the dynamics near the saddle, or near the transition state. If the reaction is influenced by processes which avoid the neighborhood of the saddle then the normal form is unlikely to capture them. One such process is corner cutting tunneling. We want to point out that the results derived from the quantum normal form, like the computation of the S -matrix and cumulative reaction probability, contain tunneling contributions, but these are related to tunneling paths which are close to the saddle. One strength of our approach is that it describes uniformly the transition from energies below the saddle energy, where only tunneling is possible, to energies above the saddle energy.

But there are situations where other tunneling contributions have a large effect. If the reaction path (e.g., the minimum energy path) in configuration space is strongly curved in the regions where it connects reactants and products, then the reactant valley and the product valley can have a small angle relative to each other. In this situation there can be quite short tunneling paths which connect reactants and products and which don't go near the saddle region. So these tunneling paths "cut the corner". The contribution from such trajectories play an important role, in particular for hydrogen exchange reactions at room temperature and lower [63].

In these situations the normal form approach has to be combined with multidimensional semiclassical tunneling calculations.

6.2 State-to-State Reaction Rates

It is important to emphasize again that, so far, our approach to quantum reaction dynamics has been local, i.e., it is derived completely from the properties of the quantum normal form that is valid in the neighborhood of the saddle-centre- \cdots -centre equilibrium point. The property of the resulting S-matrix in (4.8) being block-diagonal reflects the fact that the quantum normal form is integrable in the sense that the basis of scattering states can be chosen in the product form (4.6). In a different basis the matrix will lose this feature, and phenomena like mode mixing are related to how other incoming and outgoing scattering states are related to this special basis. It is natural to embed the study of this phenomenon in a study of the global dynamics which we will describe in this section. The global formalism is in particular required in order to compute general state-to-state reaction rates.

Let us start by describing the scattering or reaction process in classical mechanics by using Poincaré sections. Recall that a Poincaré section at energy E is given by a smooth hypersurface $\Sigma(E)$ of the energy surface with energy E which is transversal to the flow ($\Sigma(E)$ is allowed to have several components). If we have two such Poincaré sections $\Sigma_1(E)$ and $\Sigma_2(E)$ such that all the flow lines intersecting $\Sigma_1(E)$ intersect at a later time $\Sigma_2(E)$, too, then moving along the flow from $\Sigma_1(E)$ to $\Sigma_2(E)$ defines a Poincaré map

$$P^{(2,1)}(E) : \Sigma_1(E) \rightarrow \Sigma_2(E) . \quad (6.1)$$

Such Poincaré maps can be composed. If $\Sigma_3(E)$ is another Poincaré section which lies behind $\Sigma_2(E)$ in the sense that the flow lines that intersect $\Sigma_2(E)$ also intersect $\Sigma_3(E)$ at a later time, and if $P^{(3,2)}(E) : \Sigma_2(E) \rightarrow \Sigma_3(E)$ is the corresponding Poincaré map, then the Poincaré map

$$P^{(3,1)}(E) : \Sigma_1(E) \rightarrow \Sigma_3(E) \quad (6.2)$$

is given by

$$P^{(3,1)}(E) = P^{(3,2)}(E) \circ P^{(2,1)}(E) . \quad (6.3)$$

Using this construction we can describe transport through phase space regions by a sequence of maps. Given some Poincaré section $\Sigma_{\text{initial}}(E)$ located in the area of initial points in the reactants region where we prepare the system and a Poincaré section $\Sigma_{\text{final}}(E)$ in the products region where we measure the outcome, a succession of Poincaré maps

$$\Sigma_{\text{initial}}(E) \rightarrow \Sigma_1(E) \rightarrow \Sigma_2(E) \rightarrow \cdots \rightarrow \Sigma_{\text{final}}(E) \quad (6.4)$$

tells us how the initial points are transported through the system.⁹

The advantage of subdividing the flow into a sequence of maps lies in the fact that different regions in phase space might need different techniques to compute the

⁹ We here ignore the difficulties involved in constructing global Poincaré sections (see, e.g., [64]); we assume that the sequence of Poincaré sections (6.4) is intersected transversally by the trajectories with initial points from a suitable open subset in the reactants region.

flow. In our case of interest Poincaré sections can be constructed to the products and reactants side of a saddle-centre- \dots -centre equilibrium point. The dynamics ‘across’ this equilibrium point can then be described by the normal form while the dynamics between neighbourhoods of different saddle points can be obtained from integrating the original equations of motions [65, 66, 47]. Moreover, the phase space structures obtained from the local normal form can be “globalized” following the discussion in Section 2.6.

A similar procedure can be developed in the quantum case. The Poincaré maps

$$P^{(j,i)}(E) : \Sigma_i(E) \rightarrow \Sigma_j(E) \quad (6.5)$$

are symplectic maps, and as such can be quantised using the theory of Fourier integral operators. The quantisations will be unitary operators which we interpret as local S-matrices,

$$S^{(j,i)}(E) : L_{\Sigma_i(E)}^2 \rightarrow L_{\Sigma_j(E)}^2, \quad (6.6)$$

where $L_{\Sigma(E)}^2$ is a Hilbert space obtained by geometric quantisation of $\Sigma(E)$, see, e.g., [67]. This is similar to the quantisation developed in [68]. As in classical dynamics we can compose these matrices to obtain a global S-matrix

$$S^{(\text{final},\text{initial})}(E) = S^{(\text{final},n)}(E)S^{(n,n-1)}(E)\dots S^{(1,\text{initial})}(E) \quad (6.7)$$

which tells us how initial states in $L_{\Sigma_{\text{initial}}(E)}^2$ are transformed into final states in $L_{\Sigma_{\text{final}}(E)}^2$. The reasons for introducing this splitting of the S-matrix are the same as in the classical case. We can employ different techniques for computing the S-matrices according to different local properties of the system. Near equilibrium points the dynamics can be described by the quantum normal form we developed in this paper. Notice that the neighbourhoods of the saddle-centre- \dots -centre equilibrium points are the regions where we expect quantum effects to be of most importance due to partial reflection at and tunnelling through the barriers associated with saddle points. The quantum transport between neighbourhoods of different equilibrium points can be described by a standard van Vleck type formalisms, using, e.g., *initial value representations* (IVRs) which are very common in theoretical chemistry (see, e.g., [4, 69] for references).

6.3 Flux-Flux Autocorrelation Function Formalism

In this section we discuss the flux-flux autocorrelation function approach to computation of reaction rates in both classical and quantum theories.

Classical formulation: The directional flux through the dividing surface that determines the classical reaction rate, see Sec. 2.4, can be written as [8, 9, 4]

$$f(E) = \int_{\mathbb{R}^{2d}} \delta(E - H(z))F(z)P_r(z) dz. \quad (6.8)$$

The dynamical meaning of Eq. (6.8) is as follows. First, $z = (q_1, p_1, \dots, q_d, p_d)$ is a point in the system’s phase space, and the function $\delta(E - H(z))$ restricts the

integration to the energy surface of energy E under consideration. The flux factor F is given by

$$F(z) = \left. \frac{d}{dt} \Theta(s(z_t)) \right|_{t=0}, \quad (6.9)$$

where z_t is the Hamiltonian flow satisfying the initial condition $z_{t=0} = z$. The dividing surface is defined as the zero level set of the function s , i.e., $\{z \in \mathbb{R}^{2d} : s(z) = 0\}$. It is assumed that this surface divides the phase space into two components: the region given by $s(z) < 0$ corresponds to reactants, while the region given by $s(z) > 0$ to products. Finally, the projection function P_r is defined as

$$P_r(z) = \lim_{t \rightarrow \infty} \Theta(s(z_t)), \quad (6.10)$$

and equals unity (zero) if a trajectory starting at z ends up in the product (reactant) region for infinitely long times.

In order to explain the relation of Eq. (6.8) to Eq. (2.14) we first rewrite the projection function as

$$P_r(z) = \Theta(s(z_{t_0})) + \int_{t_0}^{\infty} \frac{d}{dt} \Theta(s(z_t)) dt, \quad (6.11)$$

where we choose $t_0 = -\epsilon$ with $\epsilon \rightarrow 0^+$. At this stage it is important to note that since the flux factor $F(z)$ is proportional to $\delta(s(z))$ the integral in Eq. (6.8) is effectively restricted to the dividing surface¹⁰. But, using such properties of the dividing surface that it is (i) recrossing-free and (ii) transverse to the Hamiltonian flow, we have

$$\lim_{\epsilon \rightarrow 0^+} \Theta(s(z_{-\epsilon})) = 1 - P_r(z) \quad (6.12)$$

for z on the dividing surface. Then, substituting Eqs. (6.9) and (6.12) into Eq. (6.11), and solving for the projection function P_r we obtain

$$P_r(z) = \frac{1}{2} + \lim_{\epsilon \rightarrow 0^+} \frac{1}{2} \int_{-\epsilon}^{\infty} F(z_t) dt \quad (6.13)$$

for z on the dividing surface. Finally, substituting Eq. (6.13) into Eq. (6.8), and taking into account the fact that the total flux through the dividing surface is zero, i.e.,

$$\int_{\mathbb{R}^{2d}} \delta(E - H(z)) F(z) dz = 0, \quad (6.14)$$

we arrive at the expression for the directional flux,

$$f(E) = \lim_{\epsilon \rightarrow 0^+} \frac{1}{2} \int_{-\epsilon}^{\infty} C_F(t) dt, \quad (6.15)$$

¹⁰More precisely, since in addition to the flux factor F one also has to take into account the function $\delta(E - H)$ the integral in Eq. (6.8) is a $(2d - 2)$ -dimensional integral over the intersection of the dividing surface with the energy surface of energy E .

as a time integral of the *flux-flux autocorrelation function*

$$C_F(t) = \int_{\mathbb{R}^{2d}} \delta(E - H(z)) F(z) F(z_t) dz. \quad (6.16)$$

We now explicitly calculate the time dependence of the function C_F using the classical normal form theory. To this end we first express the flux factor F in the normal form coordinates $(Q_1, P_1, q_2, p_2, \dots, q_d, p_d)$, see Sec. 2.1, in which the dividing surface is given by $s(z) = Q_1$:

$$F(z) = \left. \frac{d}{dt} \Theta(Q_1(t)) \right|_{t=0} = \delta(Q_1) \left. \frac{d}{dt} Q_1(t) \right|_{t=0} = \delta(Q_1) \Lambda P_1, \quad (6.17)$$

where

$$\Lambda = \frac{\partial}{\partial I} H_{\text{CNF}}(I, J_2, \dots, J_d) \quad (6.18)$$

and H_{CNF} is the normal form Hamiltonian as a function of the action integrals $I = (P_1^2 - Q_1^2)/2$ and $J_k = (p_k^2 + q_k^2)/2$, $k = 2, \dots, d$. Equation (6.16) then reads

$$C_F(t) = \int_{\mathbb{R}^{2d}} \delta(E - H_{\text{CNF}}) \delta(Q_1) \delta(Q_1(t)) \Lambda^2 P_1 P_1(t) dz. \quad (6.19)$$

The product of the δ -functions of Q_1 and the corresponding time evolved coordinate $Q_1(t)$ signals that only the infinitesimally short time scales $t \rightarrow 0$ give a non-vanishing contribution to the integral. Linearization the time evolution of z_t around $t = 0$ yields

$$\begin{aligned} C_F(t) &= \delta(t) \int_{\mathbb{R}^{2d}} \delta(E - H_{\text{CNF}}) \delta(Q_1) \Lambda |P_1| dz \\ &= 2\delta(t) (2\pi)^{d-1} \int_{\mathbb{R}_+^d} \delta(E - H_{\text{CNF}}) \frac{\partial H_{\text{CNF}}}{\partial I} dI dJ_2 \dots dJ_d \\ &= 2\delta(t) (2\pi)^{d-1} \int_{I(E, J_2, \dots, J_d) > 0} dJ_2 \dots dJ_d. \end{aligned} \quad (6.20)$$

The last integral in Eq. (6.20) is nothing but the volume $\mathcal{V}(E)$ in the action space (J_2, \dots, J_d) enclosed by the contour $H_{\text{CNF}}(0, J_2, \dots, J_d) = E$, and illustrated in Fig. 5, that defines the directional flux through the dividing surface, see Eq. (2.14). Thus, we obtain

$$C_F(t) = 2\delta(t) (2\pi)^{d-1} \mathcal{V}(E) = 2\delta(t) f(E), \quad (6.21)$$

which is in agreement with Eq. (6.15). Finally, we note that in view of Eq. (6.21) one can rewrite Eq. (6.15) as

$$f(E) = \frac{1}{2} \int_{-\infty}^{+\infty} C_F(t) dt. \quad (6.22)$$

Quantum formulation: In the quantum version of the flux-flux autocorrelation function approach Eq. (6.8) for the directional flux is replaced by a corresponding equation for the cumulative reaction probability,

$$\mathcal{N}(E) = 2\pi\hbar_{\text{eff}} \text{Tr} \left\{ \delta(E - \hat{H}) \hat{F} \hat{P}_r \right\}. \quad (6.23)$$

Here, the flux factor operator \hat{F} is given by

$$\hat{F} = \frac{d}{dt} \left(e^{i\hat{H}t/\hbar_{\text{eff}}} \widehat{\Theta}(s) e^{-i\hat{H}t/\hbar_{\text{eff}}} \right) \Big|_{t=0} = \frac{i}{\hbar_{\text{eff}}} [\hat{H}, \widehat{\Theta}(s)], \quad (6.24)$$

where $\widehat{\Theta}(s)$ is a quantization of the composition of the Heaviside function with a function s defining the dividing surface. The projection operator \hat{P}_r is defined as

$$\hat{P}_r = \lim_{t \rightarrow \infty} e^{i\hat{H}t/\hbar_{\text{eff}}} \widehat{\Theta}(s) e^{-i\hat{H}t/\hbar_{\text{eff}}}. \quad (6.25)$$

Then, as shown in Ref. [4], Eq. (6.23) can be written in the close analogy with its classical counterpart Eq. (6.15):

$$\mathcal{N}(E) = (2\pi\hbar_{\text{eff}}) \frac{1}{2} \int_{-\infty}^{+\infty} \mathcal{C}_F(t) dt, \quad (6.26)$$

where

$$\mathcal{C}_F(t) = \text{Tr} \left\{ \delta(E - \hat{H}) \hat{F} e^{i\hat{H}t/\hbar_{\text{eff}}} \hat{F} e^{-i\hat{H}t/\hbar_{\text{eff}}} \right\} \quad (6.27)$$

is the quantum flux-flux autocorrelation function.

As we have shown above the classical flux-flux autocorrelation function \mathcal{C}_F can be explicitly analyzed within the framework of the classical normal form theory. The following natural question arises: can one obtain the time dependence of the quantum flux-flux autocorrelation function \mathcal{C}_F using the methods of the quantum normal form theory? Of course, the QNF technique provides one with an approximation of the original Hamiltonian operator. This approximation is only accurate in the vicinity of the equilibrium saddle point in phase space, so one should not expect a perfect agreement between the QNF flux-flux autocorrelation function and the exact one to hold up to infinitely long times. Instead, the QNF theory will provide an approximation of the exact flux-flux autocorrelation function in a certain time interval whose length will depend on the effective Planck's constant among other parameters.

6.4 Convergence of Quantum Normal Form

Both the classical and quantum normal forms have the form of power series where each successive term is constructed via an iterative technique. Consequently, in general, we will only be able to compute a finite number of terms of the normal form. Therefore the obvious question that arises is how many terms of the normal form are required in order that the quantities derived from the normal form are accurate? A discussion, as well as some references with specific examples, was given in Section

2.5 for the classical normal form. In this section we are concerned with the behavior of the quantum normal form, for which there has been essentially no work from this point of view.

First, we begin with a brief background discussion. Since the normal forms, both classical and quantum, are given as series representations of the Hamiltonian function and Hamilton operator, respectively, a natural question to ask is do these series converge? In the classical setting there has been previous work on this question. However, practically speaking, from the point of view of using the results of the theory, there are three related questions: 1) convergence of the series representing the normal form Hamiltonian, 2) convergence of the transformation from the original coordinate to the normal form coordinates, and 3) convergence of any integrals of the motion that arise from the normalization procedure. A recent discussion of these issues, as well as a discussion of earlier results for the classical Hamiltonian normal form setting can be found in [70]. Briefly, the situation with respect to convergence for Hamiltonian systems with three or more degrees-of-freedom is not optimistic. Generically, divergence is the expected behavior in normal form theory for classical Hamiltonian systems. However, the situation is not so pessimistic as one may initially believe. There are many examples of divergent series which still yield useful information in an asymptotic sense. Resummation techniques and Padé approximation techniques can be used to find an optimal number of terms that yield a desired accuracy. For classical Hamiltonian normal forms these issues have been examined in [71, 72, 73, 74]. These issues have yet to be explored in the quantum normal form setting.

It is useful to note that the case of two degree-of-freedom Hamiltonian systems is special. In this case a classical result of [75] (see also [76]) gives convergence results for the classical Hamiltonian normal form in the neighborhood of a saddle-center equilibrium point. Recently, the first results on convergence of the quantum normal form have appeared. In [77] convergence results for a one and a half degree-of-freedom system (i.e. time-periodically forced one degree-of-freedom Hamiltonian system) have been given. It is not unreasonable that these results can be extended to the quantum normal form in the neighborhood of a saddle-center equilibrium point of a two degree-of-freedom system.

In the following we provide a qualitative discussion of the convergence of the QNF based on our calculations performed for the triatomic collinear reactions. In this situation the QNF approximates the Hamiltonian of the reacting system in a phase-space neighborhood of the saddle-center equilibrium point. Thus, for instance, in computing the CRP one only expects this approximation to render reliable results in a certain energy range around the saddle point energy E_0 of the potential energy surface under consideration. The energy difference $(E - E_0)$ may therefore be considered as one small parameter in the QNF expansion. The role of the other small parameter is played by the effective Planck's constant, \hbar_{eff} . It is the convergence of the QNF with respect to this second small parameter that we focus on in this section.

We proceed by considering the right hand side of Eq. (3.1), i.e., the QNF, at $I = 0$, corresponding to no "energy" in the reaction coordinate, and $n_2 = 0$, giving the zero-point 'vibrational energy' of the transverse degree of freedom. Then, Eq. (3.1)

becomes

$$E = E_0 + \sum_{n=1}^{\lfloor N/2 \rfloor} c_n \hbar_{\text{eff}}^n. \quad (6.28)$$

For the case of the collinear hydrogen exchange reaction, $\text{H} + \text{H}_2 \rightarrow \text{H}_2 + \text{H}$, on the Porter-Karplus potential energy surface the first five expansion coefficients were obtained in Ref. [31]: $c_1 = 0.161982$, $c_2 = 1.193254$, $c_3 = 14.90023$, $c_4 = 378.7950$, and $c_5 = 1227.035$. As $N \rightarrow \infty$ the radius of convergence $\hbar_{\text{eff}}^{(0)}$ of the sum in Eq. (6.28) is given by

$$\hbar_{\text{eff}}^{(0)} = \lim_{n \rightarrow \infty} \frac{c_n}{c_{n+1}}. \quad (6.29)$$

Here, we make a crude estimate of $\hbar_{\text{eff}}^{(0)}$ by only considering the first five expansion coefficients in Eq. (6.29), i.e., c_n with $n = 1, \dots, 5$; then, the radius of convergence is given by $\hbar_{\text{eff}}^{(0)} \sim 0.04$.

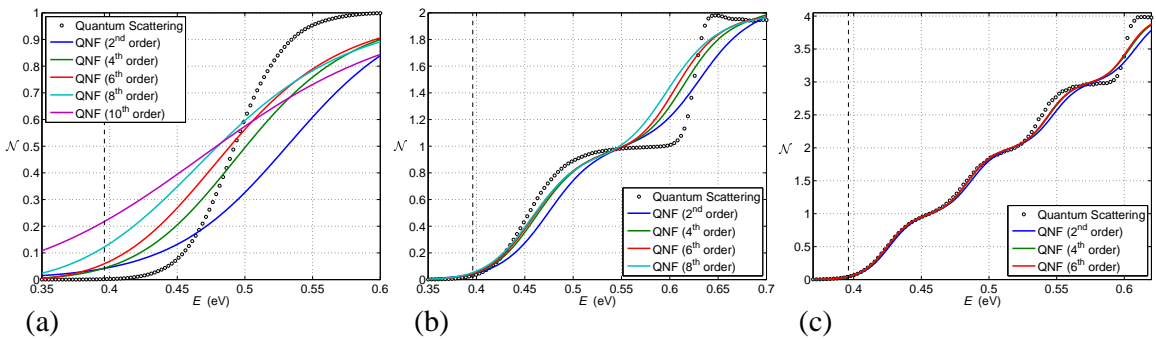


Figure 13: Cumulative reaction probability as a function of the total energy, $\mathcal{N}(E)$, for the collinear hydrogen exchange reaction. Figure (a) corresponds to ^1H isotope characterized by $\hbar_{\text{eff}} = 3.07 \times 10^{-2}$, (b) corresponds to ^3H isotope characterized by $\hbar_{\text{eff}} = 1.77 \times 10^{-2}$, and (c) corresponds to a hypothetical ^{20}H “isotope” characterized by $\hbar_{\text{eff}} = 6.9 \times 10^{-3}$. The vertical dashed line shows the saddle point energy, E_0 .

The estimated value of $\hbar_{\text{eff}}^{(0)}$ sheds light on the seeming inefficiency of the QNF theory for CRP computations in light atom reactions. Indeed, the ^1H exchange reaction, see Fig. 13a, is characterized by $\hbar_{\text{eff}} = 3.07 \times 10^{-2}$. This value being close to $\hbar_{\text{eff}}^{(0)}$ signals that the corresponding QNF expansion converges very slowly, if at all, and, possibly, terms of orders far beyond $N = 10$ are needed for a reliable CRP prediction in Fig. 13a.

In the case of the ^3H exchange reaction the effective Planck’s constant is $\hbar_{\text{eff}} = 1.77 \times 10^{-2}$ and is thus smaller than $\hbar_{\text{eff}}^{(0)}$. This fact is in agreement with the apparent speed-up of the convergence of the CRP values, see Fig. 13b, in comparison with the ^1H case. Finally, the convergence is very fast and pronounced for the case of the heavy (hypothetical) ^{20}H atoms, see Fig. 13c, for which $\hbar_{\text{eff}} = 6.9 \times 10^{-3}$ which is much smaller than the estimated convergence radius.

Clearly, there is a great deal of scope for further studies of convergence aspects of the quantum normal form as well as related optimal truncation and resummation techniques.

7 Conclusions

We have reviewed a new dynamical systems, phase space approach to quantum reactive scattering. The quantum theory arises from an underlying classical theory that reveals the geometrical structures in phase space that govern trajectories evolution from reactants to products in the reaction region. The classical theory is valid for any number of degrees-of-freedom, and the new concept which has led to this is the introduction of the notion of a *normally hyperbolic invariant manifold*, or NHIM, into classical reaction dynamics. The NHIM is the key phase space structure that leads to the construction of a surface dividing reactants from products having the no (local) re-crossing and minimal flux properties. Moreover, the stable and unstable manifolds of the NHIMs have one less dimension than the energy surface (i.e. they are “co-dimension one”) and they bound regions of the energy surface (being invariant manifolds, or “impenetrable barriers”) which contain *all* reacting trajectories. These phase space structures are realized in specific systems through the use of the classical Poincaré-Birkhoff normal form. Quantization is carried out through an analogous quantum normal form theory and the Weyl quantization procedure. The related structure of the classical and quantum normal form theories makes the quantum manifestation of the classical phase space structures transparent. The phase space structures in the classical case define the “landscape” in the *energy surface* which constrain the location and evolution of reacting trajectories, and this renders the need for the calculation of trajectories to evaluate, e.g. classical flux across the dividing surface, unnecessary. This characteristic is inherited in the quantum setting in the sense that quantum expressions governing reaction are expressed in terms of quantities that can be computed from the quantum normal form without the need to compute classical trajectories. Thus this phase space approach to quantum reactive scattering provides a completely new approach to the computation of quantities describing quantum reactive scattering which may prove to be fruitful in the study of “large” quantum systems.

Appendix

A The Normal Form Algorithm: Classical and Quantum

In Sec. 2 we mentioned that the crucial point to realize the phase space structures governing reaction dynamics is to choose a suitable set of phase space coordinates in terms of which the Hamilton function assumes a very simple form. Similarly, the description of the activated complex in Sec. 3 leading to the explicit expressions for

the cumulative reaction probabilities and the Gamov-Siegert resonances as explained in Sections 4.1 and 5, respectively, relied on expressing the Hamilton operator in a suitable basis. Both the canonical (or equivalently *symplectic*) transformation of the phase space coordinates and the corresponding transformation of the Hamilton function in the classical case, and the unitary transformation of the basis set together with the corresponding transformation of the Hamilton operator in the quantum case can be constructed in an algorithmic fashion. The algorithms are based on a (classical) *normal form* (CNF) in the classical case and on an analogous *quantum normal form* (QNF) in the quantum mechanical case. In the following we give a brief description of the algorithms to compute these normal forms. We describe the algorithms in such a way that the similarities between both algorithms become apparent. For rigorous mathematical statements, proofs and further details we refer to Ref. [29, 30].

A.1 The classical normal form algorithm

We begin by considering a Hamiltonian system with phase space $\mathbb{R}^d \times \mathbb{R}^d$ with phase space coordinates $\tilde{\mathbf{q}} = (\tilde{q}_1, \tilde{q}_2, \dots, \tilde{q}_d)$ and $\tilde{\mathbf{p}} = (\tilde{p}_1, \tilde{p}_2, \dots, \tilde{p}_d)$ which we group in the $2d$ -dimensional vector $\tilde{\mathbf{z}} = (\tilde{\mathbf{q}}, \tilde{\mathbf{p}})$, and a Hamilton function $H(\tilde{\mathbf{q}}, \tilde{\mathbf{p}})$. For convenience, we can use atomic units. This imposes no restriction. However, it has the advantage that the phase space coordinates become dimensionless. We will now assume that Hamilton's equations associated with $H(\mathbf{q}, \mathbf{p})$ have a (single) equilibrium point, $\tilde{\mathbf{z}}_0 \equiv (\tilde{\mathbf{q}}_0, \tilde{\mathbf{p}}_0)$, of saddle-center-...-center stability type. By this we mean that the matrix associated with the linearization of Hamilton's equations about this equilibrium point has two real eigenvalues, $\pm\lambda$, of equal magnitude and opposite sign, and $d-1$ purely imaginary complex conjugate pairs of eigenvalues $\pm i\omega_k$, $k = 2, \dots, d$. If the Hamilton function is of the form kinetic energy plus potential energy then this type of equilibrium point of Hamilton's equations correspond to an index one saddle point of the potential energy.

The CNF procedure consists of a sequence of canonical (or equivalently *symplectic*) transformations changing the phase space coordinates $\tilde{\mathbf{z}} = (\tilde{\mathbf{q}}, \tilde{\mathbf{p}})$ in a phase space neighborhood of the equilibrium point $\tilde{\mathbf{z}}_0$. This is accomplished order by order according to the sequence

$$\tilde{\mathbf{z}} \equiv \mathbf{z}^{(0)} \rightarrow \mathbf{z}^{(1)} \rightarrow \mathbf{z}^{(2)} \rightarrow \mathbf{z}^{(3)} \rightarrow \dots \rightarrow \mathbf{z}^{(N)}, \quad (\text{A.1})$$

where $\mathbf{z}^{(n)}$ is obtained from $\mathbf{z}^{(n-1)}$ by means of a symplectic transformation

$$\mathbf{z}^{(n-1)} \mapsto \mathbf{z}^{(n)} = \phi_{W_n} \mathbf{z}^{(n-1)}. \quad (\text{A.2})$$

generated by a homogenous polynomial $W_n(\mathbf{z})$ of order n , i.e.

$$W_n \in \mathcal{W}_{\text{cl}}^n := \text{span} \left\{ q_1^{\alpha_1} \dots q_d^{\alpha_d} p_1^{\beta_1} \dots p_d^{\beta_d} : |\alpha| + |\beta| = n \right\}. \quad (\text{A.3})$$

More precisely, the ϕ_{W_n} in (A.2) denote the time-one maps of the flows generated by the Hamiltonian vector fields corresponding to the polynomials W_n (see [30] for the

details). The maximum order N in (A.1) is the desired order of accuracy at which the expansion will be terminated and truncated.

Expressing the Hamilton function H in the coordinates $\mathbf{z}^{(n)}$, $n = 1, \dots, N$, we get a sequence of Hamilton functions $H^{(n)}$,

$$H \equiv H^{(0)} \rightarrow H^{(1)} \rightarrow H^{(2)} \rightarrow H^{(3)} \rightarrow \dots \rightarrow H^{(N)}, \quad (\text{A.4})$$

where for $n = 1, \dots, N$, and $H^{(n)}(\mathbf{z}^{(n)}) = H^{(n-1)}(\mathbf{z}^{(n-1)}) = H^{(n-1)}(\phi_{W_n}^{-1} \mathbf{z}^{(n)})$, i.e.

$$H^{(n)} = H^{(n-1)} \circ \phi_{W_n}^{-1}. \quad (\text{A.5})$$

To avoid a proliferation of notation we will in the following neglect the superscripts (n) for the phase space coordinates.

In the first transformation in (A.1) we shift the equilibrium point $\tilde{\mathbf{z}}_0$ to the origin, i.e. $\mathbf{z} \mapsto \phi_{W_1}(\mathbf{z}) := \mathbf{z} - \tilde{\mathbf{z}}_0$. This gives

$$H^{(1)}(\mathbf{z}) = H^{(0)}(\mathbf{z} + \tilde{\mathbf{z}}_0). \quad (\text{A.6})$$

The next steps of the CNF algorithm rely on the power series expansions of $H^{(n)}$,

$$H^{(n)}(\mathbf{z}) = E_0 + \sum_{s=2}^{\infty} H_s^{(n)}(\mathbf{z}), \quad (\text{A.7})$$

where the $H_s^{(n)}$ are homogenous polynomials in $\mathcal{W}_{\text{cl}}^s$ given by

$$H_s^{(n)}(\mathbf{z}) = \sum_{|\alpha|+|\beta|=s} \frac{H_{\alpha_1, \dots, \alpha_d, \beta_1, \dots, \beta_d}^{(n)}}{\alpha_1! \dots \alpha_d! \beta_1! \dots \beta_d!} q_1^{\alpha_1} \dots q_d^{\alpha_d} p_1^{\beta_1} \dots p_d^{\beta_d} \quad (\text{A.8})$$

with $\alpha_k, \beta_k \in \mathbb{N}_0$, $|\alpha| = \sum_k \alpha_k$, $|\beta| = \sum_k \beta_k$. For $n = 1$, the coefficients in (A.8) are given by the Taylor expansion of $H^{(1)}$ about the origin,

$$H_{\alpha_1, \dots, \alpha_d, \beta_1, \dots, \beta_d}^{(1)} = \prod_{k,l=1}^d \frac{\partial^{\alpha_k}}{\partial q_k^{\alpha_k}} \frac{\partial^{\beta_l}}{\partial p_l^{\beta_l}} H^{(1)}(\mathbf{z}) \Big|_{\mathbf{z}=\mathbf{0}}. \quad (\text{A.9})$$

For $n \geq 3$, the coefficients in (A.8) are obtained recursively. For $n = 2$, i.e. the second step in the sequence of transformations (A.1), the coefficients in (A.8) are determined by a linear transformation of the phase space coordinates according to

$$\mathbf{z} \mapsto \phi_{W_2}(\mathbf{z}) := M \mathbf{z}. \quad (\text{A.10})$$

Here, M is a symplectic $2d \times 2d$ matrix which is chosen in such a way that the second order term of the transformed Hamilton function

$$H^{(2)}(\mathbf{z}) = H^{(1)}(M^{-1} \mathbf{z}) \quad (\text{A.11})$$

assumes the particularly simple form

$$H_2^{(2)}(\mathbf{z}) = \lambda q_1 p_1 + \sum_{k=2}^d \frac{\omega_k}{2} (q_k^2 + p_k^2). \quad (\text{A.12})$$

Section 2.3 of Ref. [30] provides an explicit procedure for constructing the transformation matrix M .

For the first two steps in the sequence (A.1), we actually did not give explicit expressions for the generating functions W_1 and W_2 . For conceptual reasons (and to justify the notation) we mention that such expressions can be determined (see [30]) but since it is not necessary for the computation we do not discuss these generating functions here. The situation is different though for the next steps in (A.1) which rely on the explicit computation of the generating functions W_n with $n \geq 3$. In order to deal with these higher order transformations we introduce the Poisson bracket of two functions $A(\mathbf{z})$ and $B(\mathbf{z})$ which for convenience, we write as

$$\{A, B\} = A \sum_{j=1}^d \left(\overleftarrow{\frac{\partial}{\partial q_j}} \overrightarrow{\frac{\partial}{\partial p_j}} - \overleftarrow{\frac{\partial}{\partial p_j}} \overrightarrow{\frac{\partial}{\partial q_j}} \right) B. \quad (\text{A.13})$$

In this notation the arrows indicate whether the partial differentiation acts to the left (on A) or to the right (on B). With the Poisson bracket we associate the adjoint operator

$$\text{ad}_A : B \mapsto \text{ad}_A B \equiv \{A, B\}. \quad (\text{A.14})$$

The transformation (A.2) then leads to a transformation of the Hamilton function $H^{(n-1)}$ to $H^{(n)}$ with $n \geq 3$ which in terms of the adjoint operator (A.14) reads

$$H^{(n)} = \sum_{k=0}^{\infty} \frac{1}{k!} [\text{ad}_{W_n}]^k H^{(n-1)}. \quad (\text{A.15})$$

Inserting the power series for $H^{(n-1)}$ (see Equations (A.7) and (A.8)) in (A.15) and ordering terms one finds for the s^{th} order term of the power series of $H^{(n)}$:

$$H_s^{(n)} = \sum_{k=0}^{\lfloor \frac{s}{n-2} \rfloor} \frac{1}{k!} [\text{ad}_{W_n}]^k H_{s-k(n-2)}^{(n-1)}, \quad (\text{A.16})$$

where $\lfloor \cdot \rfloor$ gives the integer part of a number, i.e., the ‘floor’-function.

Using Eq. (A.16) one can show that the transformation defined by Eq. (A.15) satisfies the following important properties for $n \geq 3$. Firstly, at step n , $n \geq 3$, the terms of order less than n in the power series of the Hamilton function are unchanged, i.e.

$$H_s^{(n)} = H_s^{(n-1)}, \quad \text{for } s < n, \quad (\text{A.17})$$

so that, in particular, $H_2^{(n)} = H_2^{(2)}$. Defining

$$\mathcal{D} \equiv \text{ad}_{H_2^{(2)}} = \{H_2^{(2)}, \cdot\}. \quad (\text{A.18})$$

we get for the terms of order n ,

$$H_n^{(n)} = H_n^{(n-1)} - \mathcal{D}W_n. \quad (\text{A.19})$$

This is the so-called *homological equation* which will determine the generating functions W_n for $n \geq 3$ from requiring $\mathcal{D}H_n^{(n)} = 0$, or equivalently $H_n^{(n)}$ to be in the kernel of the restriction of \mathcal{D} to $\mathcal{W}_{\text{cl}}^n$. In view of Eq. (A.19) this condition yields

$$H_n^{(n-1)} - \mathcal{D}W_n \in \text{Ker } \mathcal{D}|_{\mathcal{W}_{\text{cl}}^n}. \quad (\text{A.20})$$

Section 3.4.1 of Ref. [30] provides the explicit procedure of finding the solution of Eq. (A.20). In the generic situation where the linear frequencies $\omega_2, \dots, \omega_d$ in (A.12) are rationally independent, i.e. $m_2\omega_2 + \dots + m_d\omega_d = 0$ implies $m_2 = \dots = m_d = 0$ for all integers m_2, \dots, m_d , it follows that for odd n , $H_n^{(n)} = 0$, and for even n ,

$$H_n^{(n)} \in \text{span} \{ I^{\alpha_1} J_2^{\alpha_2} J_3^{\alpha_3} \dots J_d^{\alpha_d} : |\alpha| = n/2 \}, \quad (\text{A.21})$$

where $I = q_1 p_1$ and $J_k = (q_k^2 + p_k^2)/2$, with $k = 2, \dots, d$.

Applying the transformation (A.15), with the generating function defined by (A.20), for $n = 3, \dots, N$, and truncating the resulting power series at order N one arrives at the N^{th} order *classical normal form* (CNF)

$$H_{\text{CNF}}^{(N)}(\mathbf{z}) = E_0 + \sum_{s=2}^N H_s^{(N)}(\mathbf{z}). \quad (\text{A.22})$$

We stress that $H_{\text{CNF}}^{(N)}$ represents an N^{th} order approximation of the original Hamiltonian H obtained from expressing H in terms of the phase space coordinates

$$\mathbf{z}^{(N)} = \phi(\tilde{\mathbf{z}}) := (\phi_{W_N} \circ \phi_{W_{N-1}} \circ \dots \circ \phi_{W_2} \circ \phi_{W_1})(\tilde{\mathbf{z}}) \quad (\text{A.23})$$

(see (A.1)). Truncating the powers series expansion of $\mathbf{z}^{(N)}$ at order N we get the transformation to the *normal form coordinates* $\mathbf{z} = (\mathbf{q}, \mathbf{p}) = T(\tilde{q}, \tilde{p})$ which we introduced in Eq. (2.1). The neighborhood \mathcal{L} of validity of the CNF is now defined as a neighborhood of the equilibrium $\tilde{\mathbf{z}}_0$ in which the difference between $H^{(N)}$ and $H_{\text{CNF}}^{(N)}$, i.e. the remainder term consisting of the nonnormalized tail of terms of order greater than N , and also the difference between the normal form coordinates \mathbf{z} and their untruncated version $\mathbf{z}^{(N)}$ can be considered to be sufficiently small for the application under consideration (see the comments in Sec. 2.5).

By construction the CNF Hamilton function $H_{\text{CNF}}^{(N)}$ is a polynomial of order $N/2$ in the functions I and J_k , see (2.4). We thus have

$$\dot{I} = \{I, H_{\text{CNF}}^{(N)}\} = 0, \quad \dot{J}_k = \{J_k, H_{\text{CNF}}^{(N)}\} = 0, \quad k = 2, \dots, d, \quad (\text{A.24})$$

i.e. I , and J_k , $k = 2, \dots, d$, are constants of the motion or *integrals* for Hamilton's equation with Hamiltonian function $H_{\text{CNF}}^{(N)}$. As discussed in Sec. 2 it is the conservation of these integrals which allows one to construct the phase space structures governing reaction dynamics in the neighborhood of the saddle equilibrium point $\tilde{\mathbf{z}}_0$. We emphasize that the full algorithm to compute $H_{\text{CNF}}^{(N)}$ and the corresponding coordinate transformation is algebraic in nature, and can be implemented on a computer.

A.2 The quantum normal form algorithm

In the quantum mechanical case we start with a Hamilton operator \hat{H} which we assume to be obtained from the Weyl quantization of a classical Hamilton function $H(\tilde{\mathbf{q}}, \tilde{\mathbf{p}})$. Like in the previous subsection, $\tilde{\mathbf{q}} = (\tilde{q}_1, \tilde{q}_2, \dots, \tilde{q}_d)$ and $\tilde{\mathbf{p}} = (\tilde{p}_1, \tilde{p}_2, \dots, \tilde{p}_d)$ denote the canonical coordinates and momenta, respectively, of a Hamiltonian system with d degrees of freedom. For convenience, we again choose atomic units, so that $\tilde{\mathbf{q}}$ and $\tilde{\mathbf{p}}$ are dimensionless. We denote the corresponding operators by $\hat{\tilde{\mathbf{q}}} = (\hat{q}_1, \hat{q}_2, \dots, \hat{q}_d)$ and $\hat{\tilde{\mathbf{p}}} = (\hat{p}_1, \hat{p}_2, \dots, \hat{p}_d)$. In the coordinate representation their components correspond to multiplication by \tilde{q}_j and the differential operators $\hat{p}_j = -i\hbar_{\text{eff}} \partial/\partial\tilde{q}_j$. Here \hbar_{eff} is a dimensionless parameter which corresponds to a scaled, effective Planck's constant (see the discussion in Sec. 3).

Like in the classical case we will now assume that $H(\mathbf{q}, \mathbf{p}; \hbar_{\text{eff}})$ (i.e. the classical Hamilton function) has an equilibrium point, $\tilde{\mathbf{z}}_0 \equiv (\tilde{\mathbf{q}}_0, \tilde{\mathbf{p}}_0)$, of saddle-center-...-center stability type. Similarly to the classical case the idea of the QNF procedure is to approximate the original Hamilton operator \hat{H} by a simpler Hamilton operator where the approximation is valid in a 'neighborhood of the equilibrium $\tilde{\mathbf{z}}_0$ '. In the classical case this simplification is achieved by a symplectic transformation leading to a specific choice of the phase space coordinates. In the quantum mechanical case the simplification will be achieved by a unitary transformation to a suitable choice of a basis for the eigenstates. The basis for computing such unitary transformation is the Wigner-Weyl symbol calculus. The crucial point of the symbol calculus is that it allows one to identify an operator with its Weyl symbol which is a (in general \hbar_{eff} dependent) phase space functions. This way the QNF theory provides a systematic procedure to obtain a local approximation, \hat{H}_{QNF} , of the Hamiltonian \hat{H} in a phase space neighborhood of the equilibrium point $\tilde{\mathbf{z}}_0$ in order to facilitate further computation of various quantities, such as the CRP, of the reaction system under consideration, which only depend on properties of \hat{H} near the equilibrium $\tilde{\mathbf{z}}_0$. From a computational point of view the symbol calculus is extremely beneficial since the resulting phase space functions can be dealt with in a similar way as in the classical case described in the previous subsection.

The Weyl symbol of an operator \hat{H} is defined as

$$H(\tilde{\mathbf{q}}, \tilde{\mathbf{p}}; \hbar_{\text{eff}}) = \int d\mathbf{x} \langle \tilde{\mathbf{q}} - \mathbf{x}/2 | \hat{H} | \tilde{\mathbf{q}} + \mathbf{x}/2 \rangle e^{i\tilde{\mathbf{p}}\mathbf{x}/\hbar_{\text{eff}}}. \quad (\text{A.25})$$

The map $\hat{H} \mapsto H(\tilde{\mathbf{q}}, \tilde{\mathbf{p}}; \hbar_{\text{eff}})$ leading to (A.25) is also called the Wigner map. It is the inverse of the transformation which yields a Hamilton operator \hat{H} from the Weyl quantization, $\text{Op}[H]$, of a phase space function H (the Weyl map) which, using Dirac notation, is given by

$$\hat{H} = \text{Op}[H] = \iint \frac{d\tilde{\mathbf{q}}d\tilde{\mathbf{p}}}{(2\pi\hbar_{\text{eff}})^d} H(\tilde{\mathbf{q}}, \tilde{\mathbf{p}}; \hbar_{\text{eff}}) \int d\mathbf{x} |\tilde{\mathbf{q}} - \mathbf{x}/2\rangle e^{-i\tilde{\mathbf{p}}\mathbf{x}/\hbar_{\text{eff}}} \langle \tilde{\mathbf{q}} + \mathbf{x}/2|. \quad (\text{A.26})$$

Accordingly, $H(\tilde{\mathbf{q}}, \tilde{\mathbf{p}}; \hbar_{\text{eff}})$ in (A.25) agrees with the classical Hamilton function $H(\tilde{\mathbf{q}}, \tilde{\mathbf{p}})$ in our case. The argument \hbar_{eff} is introduced for convenience since the Weyl symbol of the unitarily transformed Hamilton operator we will deal with below will in general explicitly depend on \hbar_{eff} .

Analogously to the classical case we will now construct a sequence of unitary transformations which will simplify the Hamilton operator order by order in the neighborhood of the equilibrium point z_0 . These unitary transformation will be of the form

$$\hat{U}_n = e^{-i\hat{W}_n}, \quad (\text{A.27})$$

where \hat{W}_n is the Weyl quantization $\text{Op}[W_n]$ of a symbol W_n which is a homogenous polynomial in the space

$$\mathcal{W}_{\text{qm}}^n := \text{span} \left\{ q_1^{\alpha_1} \dots q_d^{\alpha_d} p_1^{\beta_1} \dots p_d^{\beta_d} \hbar_{\text{eff}}^j : |\alpha| + |\beta| + 2j = n \right\}. \quad (\text{A.28})$$

The main difference between the symbols W_n and the generating functions defining the symplectic transformations in the classical case in (A.2) is that the W_n in (A.27) are polynomials in the phase space coordinates (\mathbf{q}, \mathbf{p}) and \hbar where for the definition of the order, the power of \hbar counts double.

Using unitary transformations of the form (A.27) we get the sequence of Hamilton operators

$$\hat{H} \equiv \hat{H}^{(0)} \rightarrow \hat{H}^{(1)} \rightarrow \hat{H}^{(2)} \rightarrow \hat{H}^{(3)} \rightarrow \dots \rightarrow \hat{H}^{(N)}, \quad (\text{A.29})$$

where

$$\hat{H}^{(n)} = \hat{U}_n \hat{H}^{(n-1)} \hat{U}_n^*. \quad (\text{A.30})$$

Expressing the sequence (A.29) in terms of symbols we get a sequence

$$H \equiv H^{(0)} \rightarrow H^{(1)} \rightarrow H^{(2)} \rightarrow H^{(3)} \rightarrow \dots \rightarrow H^{(N)} \quad (\text{A.31})$$

which will be the direct analogue of the classical sequence (A.4). As we will see below, in terms of the symbols the unitary transformations (A.27) can be viewed as \hbar dependent transformations of the phase space coordinates.

The first two steps of the transformations (A.31) are identical to the classical case. The first step serves to shift the equilibrium point $\tilde{\mathbf{z}}_0$ to the origin according to

$$H^{(1)}(\mathbf{z}; \hbar_{\text{eff}}) = H^{(0)}(\mathbf{z} + \tilde{\mathbf{z}}_0; \hbar_{\text{eff}}), \quad (\text{A.32})$$

The higher order transformations then work on power series expansions of the symbol of the form

$$H^{(n)}(\mathbf{z}; \hbar_{\text{eff}}) = E_0 + \sum_{s=2}^{\infty} H_s^{(n)}(\mathbf{z}; \hbar_{\text{eff}}), \quad (\text{A.33})$$

where

$$H_s^{(n)}(\mathbf{z}; \hbar_{\text{eff}}) = \sum_{|\alpha|+|\beta|+2j=s} \frac{H_{\alpha_1, \dots, \alpha_d, \beta_1, \dots, \beta_d, j}^{(n)}}{\alpha_1! \dots \alpha_d! \beta_1! \dots \beta_d! j!} q_1^{\alpha_1} \dots q_d^{\alpha_d} p_1^{\beta_1} \dots p_d^{\beta_d} \hbar_{\text{eff}}^j \in \mathcal{W}_{\text{qm}}^s. \quad (\text{A.34})$$

For $n = 1$, the coefficients in (A.34) are again given by the Taylor expansion of $H^{(1)}$ about the origin

$$H_{\alpha_1, \dots, \alpha_d, \beta_1, \dots, \beta_d, j}^{(1)} = \left(\prod_{k,l=1}^d \frac{\partial^{\alpha_k}}{\partial q_k^{\alpha_k}} \frac{\partial^{\beta_l}}{\partial p_l^{\beta_l}} \right) \frac{\partial^j}{\partial \varepsilon^j} H^{(n)}(\mathbf{z}; \varepsilon) \Big|_{(\mathbf{z}; \varepsilon) = (\mathbf{0}; 0)} \quad (\text{A.35})$$

where we included powers of \hbar only for completeness (i.e. for the type of starting classical Hamilton functions in this paper $H^{(1)}$ does not have terms with nonzero powers of \hbar). Like in the classical case the second step of the sequence of transformations (A.31) consists of a linear transformation of the phase space coordinates by a symplectic $2d \times 2d$ matrix M such that the second order term of the symbol

$$H^{(2)}(\mathbf{z}; \hbar_{\text{eff}}) = H^{(1)}(M^{-1}\mathbf{z}; \hbar_{\text{eff}}) \quad (\text{A.36})$$

takes the form

$$H_2^{(2)}(\mathbf{z}; \hbar_{\text{eff}}) = \lambda q_1 p_1 + \sum_{k=2}^d \frac{\omega_k}{2} (q_k^2 + p_k^2). \quad (\text{A.37})$$

The required matrix M is identical to the classical case.

The reason for the equality of the classical transformations and the quantum transformations to second order is the commutativity of the Weyl quantization and affine linear symplectic transformations. For the nonlinear transformations corresponding to steps $n \geq 3$ the commutativity ceases to exist and the symbol calculus develops its full power.

In order to simplify the terms of order $n \geq 3$ we have to introduce the notion of the *Moyal bracket*. Given two symbols $A(\mathbf{z}; \hbar_{\text{eff}})$ and $B(\mathbf{z}; \hbar_{\text{eff}})$, corresponding to operators \hat{A} and \hat{B} respectively, the Moyal bracket is defined as

$$\{A, B\}_M = \frac{2}{\hbar_{\text{eff}}} A \sin \left[\frac{\hbar_{\text{eff}}}{2} \sum_{j=1}^d \left(\overleftarrow{\frac{\partial}{\partial q_j}} \overrightarrow{\frac{\partial}{\partial p_j}} - \overleftarrow{\frac{\partial}{\partial p_j}} \overrightarrow{\frac{\partial}{\partial q_j}} \right) \right] B. \quad (\text{A.38})$$

The Moyal bracket gives the Weyl symbol of the operator $i[\hat{A}, \hat{B}]/\hbar_{\text{eff}}$, where $[\cdot, \cdot]$ denotes the commutator. Like in Eq. (A.13) the arrows in (A.38) indicate whether the partial differentiation acts to the left (on A) or to the right (on B). Equation (A.38) implies that for $\hbar_{\text{eff}} \rightarrow 0$,

$$\{A, B\}_M = \{A, B\} + \mathcal{O}(\hbar_{\text{eff}}^2), \quad (\text{A.39})$$

i.e. for $\hbar_{\text{eff}} = 0$, we recover the classical Poisson bracket. Moreover, if at least one of the functions A, B is a second order polynomial in the variables (\mathbf{q}, \mathbf{p}) then $\{A, B\}_M = \{A, B\}$. Analogously to the adjoint operator associated with the Poisson bracket in the classical case (see Eq. (A.14)) we now define a Moyal-adjoint operator associated with the Moyal bracket:

$$\text{Mad}_A : B \mapsto \text{Mad}_A B \equiv \{A, B\}_M. \quad (\text{A.40})$$

The symbol of $\hat{H}^{(n)}$ obtained from a unitary transformation of $\hat{H}^{(n-1)}$ according to Eq. (A.30) is then given by

$$H^{(n)} = \sum_{k=0}^{\infty} \frac{1}{k!} [\text{Mad}_{W_n}]^k H^{(n-1)}. \quad (\text{A.41})$$

Inserting the power series of $H^{(n-1)}$ and ordering terms one finds for the s^{th} order terms of the powers series of $H^{(n)}$

$$H_s^{(n)} = \sum_{k=0}^{\lfloor \frac{s}{n-2} \rfloor} \frac{1}{k!} [\text{Mad}_{W_n}]^k H_{s-k(n-2)}^{(n-1)}, \quad (\text{A.42})$$

where $\lfloor \cdot \rfloor$ again denotes the floor-function. Equation (A.42) looks formally the same as Eq. (A.16) in the classical case. The only difference is the occurrence of the Moyal adjoint operator instead of the adjoint operator associated with the Poisson bracket. This difference however is significant, as the Moyal bracket will in general introduce \hbar dependent terms although the original symbol we started with (i.e. the classical Hamilton function) had no \hbar dependence. Still, the Moyal bracket has similar properties as the Poisson bracket. Using Eq. (A.42) we see analogously the classical case that at each step $n \geq 3$, the terms of order of order less than n remain unchanged:

$$H_s^{(n)} = H_s^{(n-1)}, \quad \text{for } s < n, \quad (\text{A.43})$$

so that we in particular again have $H_2^{(n)} = H_2^{(2)}$ like in the classical case. Defining

$$\mathcal{D} \equiv \text{Mad}_{H_2^{(2)}} = \{H_2^{(2)}, \cdot\} \quad (\text{A.44})$$

we find for the terms of order n

$$H_n^{(n)} = H_n^{(n-1)} - \mathcal{D}W_n. \quad (\text{A.45})$$

This is the *quantum homological equation* which analogously to the classical case is used to determine the symbols W_n that lead to the unitary transformations \hat{U}_n defined in (A.27). Similar to the classical case we determine the W_n by requiring $\mathcal{D}H_n^{(n)} = 0$, or equivalently $H_n^{(n)}$ to be in the kernel of the restriction of \mathcal{D} to $\mathcal{W}_{\text{qm}}^n$. In view of Eq. (A.45) this condition yields

$$H_n^{(n-1)} - \mathcal{D}W_n \in \text{Ker } \mathcal{D}|_{\mathcal{W}_{\text{qm}}^n}. \quad (\text{A.46})$$

Section 3.4.1 of Ref. [30] provides the explicit procedure of finding the solution of Eq. (A.46). Provided the linear frequencies $\omega_2, \dots, \omega_d$ in (A.37) are rationally independent it again follows that for odd n , $H_n^{(n)} = 0$, and for even n ,

$$H_n^{(n)} \in \text{span} \{ I^{\alpha_1} J_2^{\alpha_2} J_3^{\alpha_3} \dots J_d^{\alpha_d} \hbar_{\text{eff}}^j : |\alpha| + j = n/2 \}, \quad (\text{A.47})$$

where $I = q_1 p_1$ and $J_k = (q_k^2 + p_k^2)/2$, with $k = 2, \dots, d$, are the analogues of the classical integrals.

Applying the transformation (A.41), with the symbol defined by Eq. (A.46), for $n = 3, \dots, N$, and truncating the resulting power series (A.33) at the N^{th} order one arrives at the Weyl symbol $H_{\text{QNF}}^{(N)}$ corresponding to the N^{th} order *quantum normal form* (QNF) of the Hamiltonian \hat{H} ,

$$H_{\text{QNF}}^{(N)}(\mathbf{z}; \hbar_{\text{eff}}) = E_0 + \sum_{s=2}^N H_s^{(N)}(\mathbf{z}; \hbar_{\text{eff}}). \quad (\text{A.48})$$

We thus see that the computation of the symbol of the QNF operator is very similar to the classical case. The major difference is the use of the Moyal bracket in the quantum case which is more complicated than the Poisson bracket in the classical case. What remains to be done to get the N^{th} order QNF operator is to compute the Weyl quantization of the symbol $H_{\text{QNF}}^{(N)}(\mathbf{z}; \hbar_{\text{eff}})$:

$$\hat{H}_{\text{QNF}}^{(N)} = \text{Op} \left[H_{\text{QNF}}^{(N)} \right]. \quad (\text{A.49})$$

The Weyl quantization of the classical integrals I and J_k , $k = 2, \dots, d$, are

$$\hat{I} \equiv \text{Op}[I] = \frac{1}{2}(\hat{q}\hat{p} + \hat{p}\hat{q}), \quad (\text{A.50})$$

$$\hat{J}_k \equiv \text{Op}[J_k] = \frac{1}{2}(\hat{q}_k^2 + \hat{p}_k^2), \quad k = 2, \dots, d. \quad (\text{A.51})$$

Using Eq. (A.37) and the linearity of the Weyl quantization we get

$$\hat{H}_2^{(2)} = \lambda \hat{I} + \sum_{k=2}^d \omega_k \hat{J}_k. \quad (\text{A.52})$$

Since the higher order terms in (A.48) are polynomials in I and J_k , $k = 2, \dots, d$ (see (A.47)), we need to know how to quantize powers of I and J_k . As shown in [30] this can be accomplished using the recurrence relations

$$\text{Op} [I^{n+1}] = \hat{I} \text{Op} [I^n] - \left(\frac{\hbar}{2} \right)^2 n^2 \text{Op} [I^{n-1}] \quad (\text{A.53})$$

and

$$\text{Op} [J_k^{n+1}] = \hat{J}_k \text{Op} [J_k^n] + \left(\frac{\hbar}{2} \right)^2 n^2 \text{Op} [J_k^{n-1}] \quad (\text{A.54})$$

for $k = 2, \dots, d$. Hence, $\hat{H}_{\text{QNF}}^{(N)}$ is a polynomial function of the operators \hat{I} and \hat{J}_k of the form Eq. (3.1). The coefficients $\kappa_{n,\alpha,j}$ are systematically obtained by the QNF procedure to compute the symbol $H_{\text{QNF}}^{(N)}$, as described above, and the recurrence relations (A.53) and (A.54). So like in the case of the classical normal form the full procedure to compute $\hat{H}_{\text{QNF}}^{(N)}$ is algebraic in nature, and can be implemented on a computer. Our software for computing the quantum normal form as well as the classical normal form which is recovered for $\hbar_{\text{eff}} = 0$ is publicly available at <http://lacms.maths.bris.ac.uk/publications/software/index.html>.

In summary the N^{th} order quantum normal form operator $\hat{H}_{\text{QNF}}^{(N)}$ is obtained from conjugating the original Hamiltonian \hat{H} by the unitary transformation

$$\hat{U} = e^{-i\hat{W}_1/\hbar_{\text{eff}}} e^{-i\hat{W}_2/\hbar_{\text{eff}}} \dots e^{-i\hat{W}_N/\hbar_{\text{eff}}}, \quad (\text{A.55})$$

where we used the fact that the first two steps in the sequence (A.31) can also be implemented using suitable generators \hat{W}_1 and \hat{W}_2 (see [30] for more details). It is an N^{th} order approximation in the sense that the symbol corresponding to the

conjugated operator is truncated at order N where the order is defined according to Eq. (A.28). Using arguments based on the symbol calculus the remainder term consisting of the Weyl quantization of the unnormalized tail $H^{(N)} - H_{\text{QNF}}^{(N)}$ is small 'in a neighborhood of the equilibrium point $\tilde{\mathbf{z}}_0$ '. The local approximation given by the QNF is ideally suited to compute the cumulative reaction probability which is directly related to properties of the Hamilton operator in the neighborhood of $\tilde{\mathbf{z}}_0$ because of the simple structure of $\hat{H}_{\text{QNF}}^{(N)}$. Since $\hat{H}_{\text{QNF}}^{(N)}$ is a polynomial function of \hat{I} and \hat{J}_k , $k = 2, \dots, d$, we have

$$[\hat{I}, \hat{H}_{\text{QNF}}^{(N)}] = 0, \quad [\hat{J}_k, \hat{H}_{\text{QNF}}^{(N)}] = 0, \quad k = 2, \dots, d \quad (\text{A.56})$$

which is the quantum analog of the invariance of the classical integrals in Eq. (A.24). The commutativities (A.56) imply that the eigenstates of $\hat{H}_{\text{QNF}}^{(N)}$ are product states of the one dimensional eigenstates of \hat{I} and the \hat{J}_k . As we demonstrated in Sections 4.1 and 5 the simplicity of the spectral properties of \hat{I} and the \hat{J}_k upon which the QNF is built can be exploited to give an efficient procedure to compute the cumulative reaction probability and the Gamov-Siegert resonances associated with the equilibrium $\tilde{\mathbf{z}}_0$.

Acknowledgments

This work was supported by the EPSRC under grant no. EP/E024629/1 and ONR under grant no. N00014-01-1-0769.

References

- [1] W. H. Miller. Using classical mechanics in a quantum framework, Perspective on "Semiclassical description of scattering" by Ford KW, Wheeler JA (1959) *Ann Phys (NY)* 7: 259. *Theor. Chem. Acc.*, 103:236–237, 2000.
- [2] W. H. Miller. The initial value representation of semiclassical theory: A practical way of adding quantum effects to classical molecular dynamics simulations of complex molecular systems. In K. K. Phua and A. Zewail, editors, *Physical Biology—From Atoms to Cells*, 51st Conference on Chemical Research, pages 505–525, London, UK, 2008. Imperial College Press.
- [3] Directing Matter and Energy: Five Challenges for Science and the Imagination. A Report from the Basic Energy Sciences Advisory Committee, US Department of Energy, December 20, 2007, 2007.
- [4] W. H. Miller. "Direct" and "Correct" Calculation of Canonical and Microcanonical Rate Constants for Chemical Reactions. *J. Phys. Chem. A*, 102(5):793–806, 1998.
- [5] G. C. Schatz and M. A. Ratner. *Quantum Mechanics in Chemistry*. Dover, Mineola, New York, 2002.

- [6] C. Venkataraman and W. H. Miller. Chemical reaction rates using the semi-classical Van Vleck initial value representation. *J. Chem. Phys.*, 126:094104, 2007.
- [7] W. H. Miller. Quantum mechanical transition state theory and a new semi-classical model for reaction rate constants. *J. Chem. Phys.*, 61(5):1823–1833, 1974.
- [8] T. Yamamoto. Quantum statistical mechanical theory of the rate of exchange chemical reactions in the gas phase. *J. Chem. Phys.*, 33(1):281–289, 1960.
- [9] W. H. Miller, S. D. Schwartz, and J. W. Tromp. Quantum mechanical rate constants for bimolecular reactions. *J. Chem. Phys.*, 79:4889–4898, 1983.
- [10] R. Collepardo-Guevara, I. R. Craig, and D. E. Manolopoulos. Proton transfer in a polar solvent from ring polymer reaction rate theory. *J. Chem. Phys.*, 128:144502, 2008.
- [11] P. Pechukas and F. J. McLafferty. On transition-state theory and the classical mechanics of collinear collisions. *J. Chem. Phys.*, 58:1622–1625, 1973.
- [12] P. Pechukas and E. Pollak. Trapped trajectories at the boundary of reactivity bands in molecular collisions. *J. Chem. Phys.*, 67(12):5976–5977, 1977.
- [13] P. Pechukas and E. Pollak. Transition states, trapped trajectories, and classical bound states embedded in the continuum. *J. Chem. Phys.*, 69:1218–1226, 1978.
- [14] E. Pollak and P. Pechukas. Unified statistical model for “complex” and “direct” reaction mechanisms: A test on the collinear $H + H_2$ exchange reaction. *J. Chem. Phys.*, 70(1):325–333, 1979.
- [15] P. Pechukas and E. Pollak. Classical transition state theory is exact if the transition state is unique. *J. Chem. Phys.*, 71(5):2062–2068, 1979.
- [16] E. Pollak, M. S. Child, and P. Pechukas. Classical transition state theory: a lower bound to the reaction probability. *J. Chem. Phys.*, 72:1669–1678, 1980.
- [17] M. S. Child and E. Pollak. Analytical reaction dynamics: Origin and implications of trapped periodic orbits. *J. Chem. Phys.*, 73(9):4365–4372, 1980.
- [18] E. Pollak and M. S. Child. Classical mechanics of a collinear exchange reaction: A direct evaluation of the reaction probability and product distribution. *J. Chem. Phys.*, 73(9):4373–4380, 1980.
- [19] S. Wiggins. On the geometry of transport in phase space I. Transport in k -degree-of-freedom Hamiltonian systems, $2 \leq k < \infty$. *Physica D*, 44:471–501, 1990.
- [20] R. E. Gillilan and G. S. Ezra. Transport and turnstiles in multidimensional hamiltonian mappings for unimolecular fragmentation: Application to van der Waals predissociation. *J. Chem. Phys.*, 94(4):2648–2668, 1991.
- [21] H. Waalkens and S. Wiggins. Direct construction of a dividing surface of minimal flux for multi-degree-of-freedom systems that cannot be recrossed. *J. Phys. A*, 37:L435–L445, 2004.

- [22] S. Wiggins, L. Wiesenfeld, C. Jaffe, and T. Uzer. Impenetrable barriers in phase-space. *Phys. Rev. Lett.*, 86(24):5478–5481, 2001.
- [23] T. Uzer, C. Jaffe, J. Palacian, P. Yanguas, and S. Wiggins. The geometry of reaction dynamics. *Nonlinearity*, 15:957–992, 2002.
- [24] H. Waalkens, A. Burbanks, and S. Wiggins. A computational procedure to detect a new type of high-dimensional chaotic saddle and its application to the 3D Hill’s problem. *J. Phys. A*, 37:L257–L265, 2004.
- [25] H. Waalkens, A. Burbanks, and S. Wiggins. Efficient procedure to compute the microcanonical volume of initial conditions that lead to escape trajectories from a multidimensional potential well. *Physical Review Letters*, 95:084301, 2005.
- [26] H. Waalkens, A. Burbanks, and S. Wiggins. A formula to compute the microcanonical volume of reactive initial conditions in transition state theory. *J. Phys. A*, 38:L759–L768, 2005.
- [27] E. Thiele. Comparison of the classical theories of unimolecular reactions. *J. Chem. Phys.*, 36(6):1466–1472, 1962.
- [28] H. Waalkens G. S. Ezra and S. Wiggins. Microcanonical rates, gap times, and phase space dividing surfaces. *J. Chem. Phys.*, 130:164118, 2009.
- [29] R. Schubert, H. Waalkens, and S. Wiggins. Efficient computation of transition state resonances and reaction rates from a quantum normal form. *Phys. Rev. Lett.*, 96:218302, 2006.
- [30] H. Waalkens, R. Schubert, and S. Wiggins. Wigner’s dynamical transition state theory in phase space: Classical and quantum. *Nonlinearity*, 21(1):R1–R118, 2008.
- [31] A. Goussev, R. Schubert, H. Waalkens, and S. Wiggins. The quantum normal form approach to reactive scattering: The cumulative reaction probability for collinear exchange reactions. *J. Chem. Phys.*, 131:144103, 2009.
- [32] H. Waalkens and S. Wiggins. Geometrical models of the phase space structures governing reaction dynamics. *Regular and Chaotic Dynamics*, 15(1):1–39, 2010.
- [33] G. S. Ezra and S. Wiggins. Impenetrable barriers in phase space for deterministic thermostats. *J. Phys. A: Math. Theor.*, 42:042001, 2009.
- [34] A. Deprit. Canonical transformations depending on a small parameter. *Celestial Mech.*, 1:12–30, 1969.
- [35] K.R. Meyer. Normal forms for hamiltonian systems. *Celestial Mech.*, 9:517–522, 1974.
- [36] A. J. Dragt and J. M. Finn. Lie series and invariant functions for analytic symplectic maps. *J. Math. Phys.*, 17:2215–2227, 1976.
- [37] V. I Arnold, V. V. Kozlov, and A. I Neishtadt. *Mathematical Aspects of Classical and Celestial Mechanics*, volume III of *Dynamical Systems*. Springer-Verlag, New York, Heidelberg, Berlin, 1988.

- [38] K.R. Meyer. A lie transform tutorial ii. In K.R. Meyer and D.S. Schmidt, editors, *Computer Aided Proofs in Analysis*, volume 28 of *The IMA Volumes in Mathematics and its Applications*, pages 190–210, New York, Heidelberg, Berlin, 1991. Springer-Verlag.
- [39] K.R. Meyer and G.R. Hall. *Introduction to Hamiltonian Dynamical Systems and the N-Body Problem*, volume 90 of *Applied Mathematical Sciences*. Springer-Verlag, Berlin, Heidelberg, New York, 1992.
- [40] J. Murdock. *Normal forms and unfoldings for local dynamical systems*. Springer-Verlag, New York, Heidelberg, Berlin, 2003.
- [41] V. Guillemin. *Moment Maps and Combinatorial Invariants of Hamiltonian T^n -spaces*. Birkhauser, Boston, 1994.
- [42] J. E. Marsden and T. S. Ratiu. *Introduction to Mechanics and Symmetry*. Springer-Verlag, New York, Heidelberg, Berlin, second edition edition, 1999.
- [43] V. I Arnold. *Mathematical Methods of Classical Mechanics*. Springer-Verlag, New York, Heidelberg, Berlin, 1978.
- [44] M. Gutzwiller. *Chaos in classical and quantum mechanics*. Springer-Verlag, New York, Heidelberg, Berlin, 1990.
- [45] R. S. MacKay. Flux over a saddle. *Phys. Lett. A*, 145:425–427, 1990.
- [46] H. Waalkens, A. Burbanks, and S. Wiggins. Phase space conduits for reaction in multidimensional systems: HCN isomerization in three dimensions. *J. Chem. Phys.*, 121(13):6207–6225, 2004.
- [47] H. Waalkens, A. Burbanks, and S. Wiggins. Escape from planetary neighborhoods. *Mon. Not. R. Astron. Soc.*, 361:763–775, 2005.
- [48] Y. Colin de Verdière and B. Parisse. Équilibre instable en régime semi-classique I. *Commun. Partial Diff. Eqns*, 19:1535–1563, 1994.
- [49] D. Chruściński. Quantum mechanics of damped systems. *J. Math. Phys.*, 44:3718–3733, 2003.
- [50] D. Chruściński. Quantum mechanics of damped systems: II. damping and parabolic barrier. *J. Math. Phys.*, 45:841–854, 2003.
- [51] M. Abramowitz and I. A. Stegun. *Handbook of Mathematical Functions with Formulas, Graphs, and Mathematical Tables*. Dover, New York, 1965.
- [52] L. M. Delves. Tertiary and general-order collisions. *Nucl. Phys.*, 9:391–399, 1959.
- [53] A. Lagana, E. Garcia, and L. Ciccarelli. Deactivation of vibrationally excited nitrogen molecules by collision with nitrogen atoms. *J. Phys. Chem.*, 91:312–314, 1987.
- [54] G. Hauke, J. Manz, and J. Römel. Collinear triatomic reactions described by polar Delves coordinates. *J. Chem. Phys.*, 73:5040–5044, 1980.
- [55] A. Kuppermann, J. A. Kaye, and J. P. Dwyer. Hyperspherical coordinates in quantum mechanical collinear reactive scattering. *Chem. Phys. Lett.*, 74:257–262, 1980.

- [56] D. E. Manolopoulos and S. K. Gray. Symplectic integrators for the multichannel schrödinger equation. *J. Chem. Phys.*, 102:9214–9227, 1995.
- [57] R. I. McLachlan and P. Atela. The accuracy of symplectic integrators. *Nonlinearity*, 5:541–562, 1991.
- [58] R. B. Walker and J. C. Lights. Reactive molecular collisions. *Ann. Rev. Phys. Chem.*, 31:401–433, 1980.
- [59] T. Seideman and W. H. Miller. Transition state theory, Siegert eigenstates, and quantum mechanical reaction rates. *J. Chem. Phys.*, 95:1768–1780, 1991.
- [60] C. Eckart. The penetration of a potential barrier by electrons. *Phys. Rev.*, 35:1303–1309, 1930.
- [61] T. Seideman and W. H. Miller. Transition state theory, Siegert eigenvalues, and quantum mechanical reaction rates. *J. Chem. Phys.*, 95:1768–80, 1991.
- [62] R. N. Zare. Resonances in reaction dynamics. *Science*, 311:1383–1385, 2006.
- [63] W. H. Miller. Semiclassical methods in chemical physics. *Science*, 233:171–177, 1986.
- [64] H. R. Dullin and A. Wittek. Complete Poincaré sections and tangent sets. *J. Phys. A*, 28:7157–7180, 1995.
- [65] S. C. Creagh. Classical transition states in quantum theory. *Nonlinearity*, 17:1261–1308, 2004.
- [66] S. C. Creagh. Semiclassical transmission across transition states. *Nonlinearity*, 18:2089–2110, 2005.
- [67] A. A. Kirillov. *Geometric quantization*, volume IV of *Dynamical Systems, Encyclopaedia of Mathematical Sciences*. Springer-Verlag, New York, Heidelberg, Berlin, 2001.
- [68] E. B. Bogomolny. Semiclassical quantization of multidimensional systems. *Nonlinearity*, 5:805–866, 1992.
- [69] W. H. Miller. Spiers Memorial Lecture. Quantum and semiclassical theory of reaction rates. *Farad. Discuss.*, 110:1–21, 1998.
- [70] R. Pérez-Marco. Convergence or generic divergence of the Birkhoff normal form. *Annals of Mathematics*, 157:557–574, 2003.
- [71] M. Kaluza and M. Robnik. Improved accuracy of the Birkhoff-Gustavson normal form and its convergence properties. *J. Phys. A: Math. Gen.*, 25:5311–5327, 1992.
- [72] M. Robnik. On the Padé approximations to the Birkhoff-Gustavson normal form. *J. Phys. A: Math. Gen.*, 26:7427–7434, 1993.
- [73] G. Contopoulos, C. Efthymiopoulos, and A. Giorgilli. Non-convergence of formal integrals of motion. *J. Phys. A: Math. Gen.*, 36:8639–8660, 2003.
- [74] C. Efthymiopoulos, A. Giorgilli, and G. Contopoulos. Nonconvergence of formal integrals: II. Improved estimates for the optimal order of truncation. *J. Phys. A: Math. Gen.*, 37:10831–10858, 2004.

- [75] J. Moser. On the generalization of a theorem of A. Liapounoff. *Comm. Pure Appl. Math.*, 11:257–271, 1958.
- [76] A. Giorgilli. Unstable equilibria of hamiltonian systems. *Discr. Cont. Dyn. Sys. (DCDS-A)*, 7(4):855–871, 2001.
- [77] A. Anikin. Normal form of a quantum Hamiltonian with one and a half degrees of freedom near a hyperbolic fixed point. *Regular and Chaotic Dynamics*, 13:377–402, 2008.